Pure Appl. Geophys.

https://doi.org/10.1007/s00024-024-03476-2

Pure and Applied Geophysics

Investigation of Atmospheric Anomalies due to the Great Tohoku Earthquake Disturbance Using NRLMSISE-00 Atmospheric Model Measurement

Lake Endeshaw[1,2]

Abstract—In this study, the atmospheric changes for the 9.0-magnitude Tohoku earthquake, which occurred on March 11, 2011, are analyzed. The March 11, 2011 earthquake was preceded by a large foreshock on March 09, 2011 with magnitude M 7.3 and depth 32 km at 02:45:20 UT near the east coast of Honshu, Japan. The earthquake doesn't limit its effects on the Earth's lithosphere, hydrosphere and biosphere; it also extends its effects to the atmosphere because of the gas emissions, which produce large-scale seismic waves from the ground and release gases into the atmosphere. In this study, the anomalies of the atmospheric parameters are studied by using one of the atmospheric models from the Naval Research Laboratory Mass Spectrometer Incoherent Scatter Extension 2000 (NRLMSISE-00) model data to analyze the atmospheric anomalies of the Tohoku Earthquake on March 11, 2011. The atmospheric parameters of atomic oxygen (O), hydrogen (H), atomic nitrogen (N), helium (He), argon (Ar), molecular oxygen (O_2), molecular nitrogen (N_2), total mass density (ρ), neutral temperature (Tn), exospheric temperature (Tex) and anomalous oxygen (AO) are used for analysis during the earthquake occurrence. The epicenter of the Tohoku earthquake, with a geographical location of latitude 38.30° N and longitude 142.37° E, is used for the NRLMSISE-00 model as input parameters to analyze the output of atmospheric parameters. To compare the atmospheric changes caused by the earthquake, 5 days before and after the earthquake are considered. To detect where the atmospheric parameters increased or decreased from the earthquake day, the percentage deviation of the NRLMSISE-00 model is applied. The results indicate that there were atmospheric parameter anomalies that occurred a few days before, following and during the earthquake on March 11, 2011. Except for hydrogen (H), all atmospheric parameters average daily percentage deviation values were positive during the 5 days before and after with respect to the main earthquake shock on March 11, 2011. The NRLMSISE-00 model can capture the atmospheric parameter anomalies of the Tohoku earthquake well.

Keywords: Atmospheric anomalies, Atmospheric parameters, Earthquake, NRLMSISE-00 model, Percentage deviation.

1. Introduction

An earthquake is a natural phenomenon that has been occurring for billions of years on our planet. Many reports from man's history demonstrate the significant impact they have had on human lives and property. Earthquakes are one of the most terrifying and destructive natural phenomena. The moment an earthquake occurs, the outermost layer of earth shakes, causing ground rupture, landslides, avalanches, fires, the destruction of forests, and significant building damage. Generally, the earthquake has effects on the geosphere, biosphere, hydrosphere, atmosphere and society (Al-Taie & Albusoda, 2019). The Mw 9.0 Tohoku earthquake that struck mainland Japan on March 11, 2011 caused a devastating tsunami due to active thrusting between the Pacific and North American Plates (Param et al. 2019). This event's hypocenter was at the juncture of four tectonic plates and comprehensive understanding is still a source of debate. Several models have been proposed and referred to (DeMets, 1992a, 1992b; Seno et al., 1996) regarding plate limits and their role in shaping regional kinematics following the Tohoku event, particularly the exact location of the limits around Honshu Island's focal zone (Seno et al., 1996).

What is still unknown is the impact of the Tohoku earthquake's atmospheric changes around on the epicentre. The operational and upper atmospheric research communities rely on empirical thermosphere and mesosphere models for data analysis, the initialization of detailed physics-based models, and mission and instrument design. The Mass Spectrometer Incoherent Scatter (MSIS-class) Radar model, which is derived from the Drag Temperature Model

[1] Department of Physics, Werabe University, Werabe, Ethiopia. E-mail: endeshawlake@gmail.com
[2] Department of Space and Planetary Science, Ethiopian Space Science and Geospatial Institute, Entoto Observatory and Research Center, Addis Ababa University, Addis Ababa, Ethiopia.

Published online: 16 April 2024

(DTM), is one of the most commonly used atmospheric empirical models. The MSIS-class model is being improved in various ways. Hedin et al. (1977) introduced the first version of MSIS-class models (MSIS-1) in 1977, using temperature and composition measurement data with a lower boundary of 120 km. The MSIS-1 model has flaws under high solar activity conditions because the data used to develop it were mostly collected under low to moderate solar activity conditions and only a few were collected under high solar activity conditions ($F10.7 > 170$ SFU). Furthermore, the MSIS-1 model's lower formal boundary is 120 km. In 1983, Hedin (1983) created the MSIS-83 model, which lowered the boundary to 90 km and included data from rocket flights, seven satellites, and five incoherent scatter radars, as well as data from high solar activity. In addition to the daily geomagnetic activity index, ap, the MSIS-83 model used an alternate representation of geomagnetic activity (three hourly ap indices). Hedin (1987) developed the MSIS-86 model to improve the representation of polar region morphology by adding or changing terms to better represent seasonal variations in the polar regions. The MSISE-90 model extended the lower limit of the MSIS-class model to the Earth's surface (Hedin, 1991). Picone et al. (2002) established the MSIS class model for the Naval Research Laboratory's MSIS Extension 2000 (NRLMSISE-00) model, which includes total mass density data from satellite accelerometers and orbit determination, recent temperature data from incoherent scatter radar, and molecular oxygen number density data from the Solar Maximum Mission's (SMM) solar ultraviolet occultation.

The NRLMSISE-00 model has an alternate representation of geomagnetic storm behaviors that uses a formula based on 3 h ap indices as well as the daily Ap geomagnetic index. The NRLMSISE-00 is an empirical model that extends from the ground to the exobase and is commonly used as a model comparison standard (Hedin, 1991; Picone et al., 2002). The Mass Spectrometer Incoherent Scatter model has been steadily improved as MSIS-1 (Hedin et al., 1977) in 1977, MSIS-83 (Hedin, 1983) in 1983, MSIS-86 (Hedin, 1987) in 1987, MSISE-90 (Hedin, 1991) in 1991, and NRLMSISE-00 (Picone et al., 2002) in 2001. Several studies and efforts on the NRLMSISE-00 model have been conducted over the last decade, including (Chen et al., 2013a, 2020; Mehta & Linares, 2017; Zhang et al., 2018; Perez & Bevilacqua, 2015; Xiong et al., 2018; Pederick & Cervera, 2014; Shi et al., 2015; Bruinsma & Boniface, 2021; Emmert, 2015; Nossal et al., 2012; Kotov et al., 2018; Calabia et al., 2019). In recent years, many researchers have focused their efforts on estimating and mitigating ionospheric time delays using standard models (Astafyeva, 2019; Conker et al., 1997; De Santis et al., 1994; Lejeune & El-Arini, 1999; Sahithi et al., 2019; Sparks et al., 2000; Walter et al., 2000).

Many studies on earthquake sequences and anomalies have been conducted using various methods of satellite and ground observations. Sano et al. (2014) evaluated the geochemical nature and behavior of pore fluids along the interface between the two plates of the Pacific and the Okhotsk. They concluded that the helium isotopes were useful in identifying the origin of fluids and may provide key information about the source of interplate fluids and a sudden emanation of mantle helium related to an interplate earthquake in the subduction zone, which may provide insight into the movement of mantle-derived fluids. Sahithi et al. (2019) used the Extended Single Layer Model (ESLM) with the planar fit (PF) and the spherical harmonic function (SHF) techniques to estimate ionospheric time delays from a regional network of TEC data over the equatorial Indian Subcontinental region. Afraimovich et al. (2006) proposed a secondary source above the epicenter and located it at the height of the maximum ionization by using the 2000 Mw 7.7 Sumatra earthquake. Liu et al. (2010) used a grid search to minimize the differences in apparent velocities between multiple satellite-station pairs' observed Co-seismic-Ionospheric-Disturbance (CID). They located the source of the 1999 Mw 7.6 Chi-Chi earthquake between 40 and 130 km north of the epicenter and demonstrated that the origin of the ionospheric disturbance is near the maximum of surface deformation, not at the epicenter. Lee et al. (2018) used the seismologically derived technique of back-projection to locate the acoustic source of the 2016 Mw 7.8 Kaikoura earthquake. Zedek et al. (2021) assessed TEC data from two

earthquakes with different moment magnitudes: a Mw 7.1 in Turkey and a Mw 7.8 in New Zealand and they conclude that a sparse network of multi-GNSS stations can provide an independent estimation of the spatial distribution of large scale coseismic motions, including offshore areas 200–300 km from the coast. Ahmed et al. (2022) studied the ionospheric perturbation in the form of enhancement and depletion of the critical frequency of the F2 layer before the M5.6 magnitude earthquake in Pakistan. Parrot et al. (2006) investigated anomalies in ion composition, electron density, and ion temperature over seismic breeding regions in long-term DEMETER (Detection of Electro-Magnetic Emissions Transmitted from Earthquake Regions) satellite data. Similarly, Shah et al. (2019) investigated DEMETER satellite and in situ GNSS observations for monitoring large magnitude earthquakes for possible ionospheric perturbations in order to provide evidence for Lithosphere-Atmosphere–Ionosphere Coupling (LAIC). Maruyama et al. (2011) described the effect of earthquake on ionosphere disturbances using ionosonde stations. Similar observations of a sudden decrease in TEC as the ionosphere's response to the earthquake/tsunami were reported by Saito et al. (2011) and Tsugawa et al. (2011).

An earthquake is a natural phenomenon that has varied associations between different parts of the earth and the sun. For instance, with the lithosphere (Pulinets et al., 2006; Sharzehei et al., 2015), atmosphere (Bokov, 2004; Heki, 2011; Dimitar et al., 2011; Ohta et al., 2013; Hayakawa & Hobara, 2010; Maruyama et al., 2011; Freund et al., 2022; Kavanagh et al., 2018; Kutoglu et al., 2021), ionosphere (Le et al., 2011, 2013; Zhou et al., 2017; Liu et al., 2006; Ryu et al., 2016), solar magnetosphere (Khachikyan et al., 2012; Wang et al., 2022), internal and external of the Earth system (Chen et al., 2020; Akhoondzadeh & Santis, 2022), space weather phenomena (Temmer, 2021), solar activities (Odintsov et al., 2007; Le et al., 2013; Takla & Samwel, 2023), geomagnetic storm (Moldovan et al., 2012; Le et al., 2013; Love & Thomas, 2013; Yesugey, 2009; Guglielmi et al., 2020, 2021; Sobolev & Zakrzhevskaya, 2020; Sobolev, 2021); coronal mass ejection (Anagnostopoulos et al., 2021), cosmic ray intensity (Yanchukovsky, 2020), geomagnetic activities index (Urata et al., 2018; Guglielmi et al., 2020; Shah et al., 2020a), atmospheric waves (Guglielmi & Klain, 2020), sunspots numbers (Odintsov et al., 2006; Sukma & Dbidin, 2017), air temperature (Mahmood et al., 2017), underground pressure (Mahmood et al., 2017), air conductivity (Kavanagh et al., 2018), Earth's particle radiation (Vainio et al., 2009), atmospheric temperature (Alimov et al., 1989), infrared long-wave (Zhu et al., 2023), neutral temperature (Arai et al., 2011; Freund et al., 2022; Kakinami et al., 2021) and solar wind and interplanetary magnetic field (Guglielmi et al., 2020).

Earthquakes have an impact on the earth's environment, including but not limited to ionospheric perturbations in the lower ionosphere (Hayakawa & Hobara, 2010; Maruyama et al., 2011), upper ionosphere (Liu et al., 2006; Ryu et al., 2016), geomagnetic field variations (Khachikyan et al., 2008, 2012; Wang et al., 2022), TEC variations (Jin et al., 2015), and solar magnetosphere variations (Khachikyan et al., 2012; Wang et al., 2022). The majority of studies (Jin et al., 2015; Shah et al., 2020a) report ionospheric anomalies some days before and after the main shock of various earthquakes in the seismogenic zone. For instance, within 5–10 days after the primary shock, Shah et al. (2020b) investigated long-term ionosphere data over earthquake-preparation zones and found both positive and negative anomalies. Different reports on global and regional scales investigate earthquake-induced ionospheric and atmospheric anomalies by employing various methods for monitoring the epicentral regions (Tariq et al., 2020; Shah, 2022; Satti et al., 2022; Shah et al., 2020C; 2021; Shah & Jin, 2018; Perrone et al., 2010; Heki, 2011; Yang et al., 2019a).

A detailed analysis by Le et al. (2013) of the ionospheric anomalies was presented three days before the 9.0-magnitude Tohoku earthquake on March 11, 2011. They concluded that the solar and geomagnetic activities were not enough to cause the observed ionospheric increases for a long time, and these regional anomalies might be related to the greatest earthquake in Tohoku. Similarly, more investigation into atmosphere parameters related to this extreme earthquake is needed (Heki, 2011; Freund et al., 2022).On the basis of the atmospheric changes given for the 9.0 magnitude earthquake in

the great Tohoku Earthquake that occurred on March 11, 2011, there is a limitation to the study of atmospheric parameters in the evaluation of earthquake hazard. As a result, it is crucial to study the atmospheric anomalies during the earthquake and the purpose of this paper is to investigate the effect of the earthquake on the Earth's atmosphere using one of the atmospheric models from the NRLMSISE-00 model.

1.1. The Atmospheric Parameter Anomalies and the NRLMSISE-00 Model

The NRLMSIS-00 atmospheric model estimates the average observed behavior of temperature, eight species densities (N_2, O_2, O, He, H, Ar, N, and anomalous O), and total mass density as a function of location, day of year, time of day, solar activity and geomagnetic activity (Kotov et al., 2023). Temperature: Atmospheric parameters and mass densities are highly sensitive to the entire thermospheric temperature profile, and any temperature measurements during periods of different disturbances are very important (Kotov et al., 2023). Because of these issues, the temperature behavior of the atmosphere during the earthquake period is included in this study. Molecular Nitrogen: Nearly eighty percent of the gases in the atmosphere are made up of molecular nitrogen (N2). Atomic nitrogen and its species are the most important in the Earth's atmosphere and have a significant role in determining the atmosphere's structure (Emmert et al., 2022). The mass density is significantly influenced by N2. Molecular Oxygen: Approximately 21% of the earth's atmosphere is made up of molecular oxygen (O2). And also, the density of atomic Oxygen (O) in the thermosphere and exosphere influences the flow of plasma into the plasmasphere after different disturbances (Krall et al., 2018). Atomic Oxygen: Atomic Oxygen (O) is likely the most essential and challenging species to represent in upper atmospheric applications. At thermospheric altitudes, O is the main neutral element of the atmosphere and the principal source atom for F region ionization. However, O is a minor element in the mesosphere and lower thermosphere and is subject to photochemical production and loss, dynamical movement, and diffusion. O is critical in calculating the energy budget at the mesopause (Mlynczak and Solomon, 1993). NRLMSISE-00 and previous versions accurately represented thermospheric O from mass spectrometer data (Emmert et al., 2020). The $O+ + H$ reaction causes a somewhat decrease in $O+$ density while increasing H density. This impact, however, is significantly less than the loss of $H+$ caused by the upward flow. As a result, when the daytime H density increases, the difference between the $H+$ and $O+$ densities grows, resulting in a significant sensitivity of the daytime $O+/H+$ transition height to the H density (Kotov et al., 2023; Qian et al., 2018).

Atomic Hydrogen: One of the important aspects of the atmosphere is the variability of atomic Hydrogen (H). Mlynczak et al. (2014) highlight an inverse interaction between lower thermosphere H and solar activity, which is an interesting feature. Krall et al. (2018) investigated atomic Hydrogen's space weather consequences during the period of disturbance. They demonstrated that the ring current associated with a geomagnetic storm decays faster as H increases and that it has a close relationship with the geomagnetic field lines. As a result, there may be atomic Hydrogen abnormalities during earthquake times (Picone et al., 2002; Qin & Waldron, 2016; Qian et al., 2018). Understanding H and its fluctuation will help researchers understand more about the Earth's temperature, magnetosphere and plasmasphere, and water budget. As a result, it is critical to enhance our existing understanding of hydrogen variability and the empirical definition of hydrogen variability in NRLMSISE-00 (Kotov et al., 2023; Qian et al., 2018). This study assesses the significance of anomalies in H density for atmospheric dynamics, which will be of interest to scientists and program managers working on establishing the next generation of space weather prediction models.

Total mass density (ρ): The atmospheric total mass density (ρ) depends on its temperature, pressure, and the amount of water vapor in the atmosphere. Because of the gravity of the earth, air density decreases with height, and this vertical variation is significantly greater than the horizontal gradient. The molecules of nitrogen, oxygen, and other gases that constitute air move at high rates of speed, interacting with one another and all other

objects. The faster the molecules move, the higher the temperature (Zhang et al., 2021; Seemala, 2023). Since the earthquake disturbance caused or effected anomalies in the atmospheric parameters (Heki, 2011; Mahmood et al., 2017; Yanchukovsky, 2020; Freund et al., 2022), there were also anomalies in the atmospheric total mass density during the earthquake period. One of the most significant factors influencing spacecraft orbital precision in low Earth orbit (LEO) is the accuracy of air mass density. While there are several empirical density models available for use in determining and predicting the orbits of LEO spacecraft, all of them include discrepancies of varying magnitudes. This parameter is better determined using the NRLMSISE-00 atmospheric model, based on densities obtained from space-borne accelerometer data (Zhang et al., 2021).

1.2. The Atmospheric Parameter Anomalies and Earthquake Precursors

Earthquake precursors tend to be found in three regions: the surface precursors, the atmosphere precursors, and the ionosphere precursors. This section analyzes the relationship between the atmospheric parameter anomalies and the precursors of the earthquake. Air temperature: This shows how seismic activity in the atmosphere reacts to atmospheric parameters and helps us understand the atmospheric phenomena related to the main shock (Draz et al. 2023; Heki, 2024). Refractivity: Radio refractivity is the bending of radio signals, and it is crucial to the point-to-point atmospheric electromagnetic propagation of microwave communication, television and radio broadcasts, WiFi signals, mobile communication systems, and the investigation of how satellite signals travel through the atmosphere. According to Emmanuel et al. (2017), Agbo et al. (2021), Abimbola et al. (2021), Cheloni et al. (2024), and other atmospheric factors, radio-refractivity and atmospheric temperature, pressure, and water vapor concentration are correlated with each other most of the time. Relative humidity: The term atmospheric relative humidity refers to the ratio between the vapor pressure of the air and its saturation vapor pressure. Additionally, relative humidity is required for the formation of meteorological disturbances (North et al., 2014; Sherwood et al., 2010). Relative humidity status is a key factor in global energy exchange, atmospheric dynamics, earthquake-related atmospheric reactivity, and troposphere-stratosphere interaction surrounding the epicenter (Heki, 2024). Water vapor: The primary component of greenhouse gases in the atmosphere, water vapor, has highly variable distributions. The hydrological cycle, the climate system, and the global energy budget are all significantly impacted by the thermodynamic and radiative characteristics of water vapor. Increasing atmospheric water vapor is responsible for a considerable portion of the Earth's temperature rise brought on by increasing greenhouse gas concentrations in the atmosphere (Price et al., 2023). Moreover, water vapor is essential to atmospheric chemistry because it facilitates several processes that purge the atmosphere of pollutants. Raising temperatures lead to a rise in the lower troposphere's concentration of water vapor, which in turn accelerates the rate of evaporation and increases the amount of water vapor in the atmosphere. This generally results in greater warming and has an additional impact on the atmospheric parameter anomalies (Shao et al., 2023).

Radon: The radioactive gas radon is colorless, odorless, and tasteless. The naturally occurring radioactive decay of uranium, which is present in all rocks, soils, and water, produces radon. Worldwide observations have shown that upcoming geophysical events, such as earthquakes or volcanic activity, might intensify radon emissions. The radon abnormalities that have been found in soil, gas, or groundwater are a symbol of earthquakes. It is simple to identify the presence as well as the amount of radon, which is a significant terrestrial gas. Radon concentration measurements in the earth's crust have long been conducted in the hopes of identifying distant sources or understanding the mechanisms underlying gas release. It is anticipated that the strain changes that take place within the earth's surface during an earthquake will increase the amount of radon in soil gas. But geological, geophysical, and atmospheric factors like rainfall and pressure have a significant impact on radon concentration levels. Because temperature, precipitation, and atmospheric pressure are all interrelated components of atmospheric parameters, the radon concentration also

relates to these parameters (Ghosh et al., 2009). When radon departs the earth and enters the atmosphere, it decays and releases more radioactive particles. Seismic activity in a geothermal environment modifies fluid convective fluxes and rock pressures. Changes in gas transportation and the ascent of volatiles from the deep earth to the surface are caused by the stress strain that develops inside the crust of the earth prior to an earthquake. Because of this, radon leaks out of the pores and surface cracks of the rocks in unusually high amounts. Anomalous radon concentration anomalies and other short- and long-term precursory events are invariably linked to earthquake deformations. Both soil gas and groundwater have had their radon concentrations vary. However, it is also important to keep in mind that radon anomalies are influenced by a variety of meteorological parameters, including soil moisture, rainfall, temperature, air pressure, and others, and are not only determined by earthquakes (Ghosh et al., 2009). Radio waves: Waves that are borne via electromagnetic field sources are known as radio waves. They are generated by electric charges undergoing a change in velocity with respect to time. In the lower atmosphere, changes in the refractive index of air are key in the determination of radio wave propagation. Radio waves refract towards the earth's surface with a curvature that exceeds the curvature of the earth (Cheloni et al., 2024). *Precipitation:* There are multiple links between precipitation and atmospheric parameters associated with precipitation. One popular method for dealing with precipitation is to merge snowfall and rainfall into one data type (Walsh et al., 2022). Atmospheric electric field: anomalies in the atmospheric electric field are seen after earthquakes. The probable reason for the observed anomalies in the atmospheric electric field is that internal gravity waves, which were produced in the vicinity of the EQ epicenter several hours before the EQ, crossed the field site and altered the atmospheric electric field by altering the density of space charges in the uppermost layer of the atmosphere. Seismo-electromagnetics, or electromagnetic phenomena related to earthquakes, have been observed to manifest as short-term EQ precursors before an earthquake. These phenomena are observed not only in the lithosphere but also in the atmosphere and ionosphere. Even in this scenario, there is still debate on short-term EQ precursors because there is insufficient evidence to link those anomalies to EQs (Hobara et al., 2022). Solar activity: There have been several known or postulated precursors to seismic risks, and more recently, the Sun's solar activity has been mentioned as a potential influencing factor of the Earth's seismicity (Junqueira & Hirata, 2022).

2. *Data and Method of Analysis*

In this study, the anomalies of the atmosphere are studied by using one of the atmospheric models of the NRLMSISE-00 model data to analyse the atmospheric anomalies of the Tohoku Earthquake on March 11, 2011. The atmospheric parameters of atomic oxygen (O), hydrogen (H), atomic nitrogen (N), helium (He), argon (Ar), molecular oxygen (O_2), molecular nitrogen (N_2), total mass density (ρ), neutral temperature (T_n), exospheric temperature (T_{ex}) and anomalous oxygen (AO) are used for analysis during the earthquake disturbance. The epicenter of the Tohoku Earthquake, with a geographical location of latitude 38.30° N and longitude 142.37° E, is used for the NRLMSISE-00 model as input parameters to analyze the output of atmospheric parameters. To compare the atmospheric changes caused by the earthquake, five days before and after the earthquake are considered. To detect where the atmospheric parameters are increased or decreased from the earthquake day, the percentage deviation of the NRLMSISE-00 model is applied. The anomalies of the atmospheric parameters are estimated by the following formula:

$$\text{Anomalies deviation } (\%) = \frac{EQ - EQbf/af}{EQ} \times 100, \quad (1)$$

where, EQ-Earthquake parameters on March 11, 2011 and EQbf/af—days before or after the earthquake parameters from March 11, 2011 The anomaly percentage deviation is the value of the difference between before or after the main earthquake parameter and the main earthquake parameter divided by the main earthquake parameter values times 100. The positive anomaly percentage deviation indicates the

values of the atmospheric parameters during the main earthquake on March 11, 2011 were higher than days before or after the main earthquake parameter values. The inverse is true for the negative anomalies percentage deviation. Five days before (March 06–10, 2011) and after (March 12–16, 2011), the main earthquake shock of the March 11, 2011 earthquake is used as the hourly and daily average (calculated from the hourly percentage deviation of each day) of anomalies percentage deviation. According to the description of Picone et al. (2002), in the NRLMSISE-00 model, all eleven atmospheric parameters are fully available at high altitudes, and in this study, an altitude of 500 km is selected (Picone et al., 2002; Piscini et al., 2017; Reber et al., 1973). The year, month, day, time (UT/LT), altitude, geographic/geomagnetic location, and solar and geomagnetic activities are used as the model input variables (Ahmed et al., 2022; Picone et al., 2002).

3. Results

During the earthquake preparation period, there are various methods for detecting ionospheric and atmospheric anomalies before and after the main shock. These anomalies have been classified as either positive/increase or negative/decrease on a given day based on the background data (Shah and Jin 2018). An anomaly beyond upper confidence bounds can be positive, while an anomaly below lower confidence bounds is negative (Perrone et al., 2010). On March 11, 2011, a megathrust off the east coast of Honshu, Japan, reported a significant deviation in total electron content data from the GPS approximately 40 min before the event (Heki, 2011). As shown in the figures below, to compare the atmospheric parameter changes caused by the earthquake, five days before and after the earthquake are considered. From Fig. 1, the atomic oxygen (O) starts increasing from March 06 to March 11, 2011 and then decreases after March 11, 2011, so O got its highest value of 2.957E + 07 at 5:00 UT during the March 11, 2011 earthquake and its lowest value of 4.377E + 06 at 18:50 UT during the March 16, 2011. The percentage deviation in O variation on the March 11, 2011 earthquake is shown in Fig. 1 and Table 2. The molecular oxygen shows a similar pattern as the atomic oxygen and has a percentage deviation value variation from the March 11, 2011 earthquake. The highest and lowest values of molecular oxygen are 1.032E + 04 at 5:50 UT on March 11, 2011 and 1.469E + 02 at 19:00 UT on March 16, 2011, respectively. According to Fig. 1 and Table 2, the hydrogen (H) has a percentage deviation variations on March 11, 2011, decreases in value before and after the main earthquake shock. The H has a maximum value of 2.637E + 05 at 17:00 UT on March 16, 2011 and a minimum value of 8.532E + 04 at 7:00 UT on March 11, 2011. The helium (He) atom shows greater values in the days before and after the main earthquake shock, especially in the hours from 2:00 UT to 18:00 UT. The highest and lowest values of the He atom are 4.170E + 06 at 22:00 UT on March 09, 2011 and 1.865E + 06 at 10:00 UT on March 16, 2011, respectively. The atomic nitrogen (N) exhibits variability with values on March 11, 2011, the major earthquake shock, with five days before and decreasing with values after the main earthquake days. In Fig. 1 and Table 2, the percentage deviation values for the March 11, 2011 earthquake and non-earthquake events are presented. The N has a maximum value of 1.297E + 06 at 04:00 UT on March 11, 2011 and a minimum value of 1.025E + 05 at 22:50 UT on March 16, 2011. Similarly, molecular nitrogen (N2) shows the same trend with values of the percentage deviation and got its highest value of 5.979E + 05 at 5:50 UT on March 11, 2011 and its lowest value of 1.493E + 04 at 19:00 UT on March 16, 2011.

As shown in Fig. 2, the argon (Ar) value on March 09, 2011 was the highest of all days, especially before around 8:00 UT with its peak value of 1.064E + 01 at 5:50 UT and its lowest value of 4.282E-02 at 19:00 UT on March 16, 2011. The neutral temperature (Tn) varies in values from the days prior, during and after the earthquake on March 11, 2011, as shown in Fig. 2 and Table 2, with its highest value of 1081.8 at 6:50 UT on March 09, 2011 and its lowest value of 752.1 at 18:50 UT on March 16, 2011. In a similar trend, the exospheric temperature (Tex) has similar values with percentage deviations shown in Fig. 2 and Table 2, with its highest value of 1083 at 6:50 UT on March 09, 2011

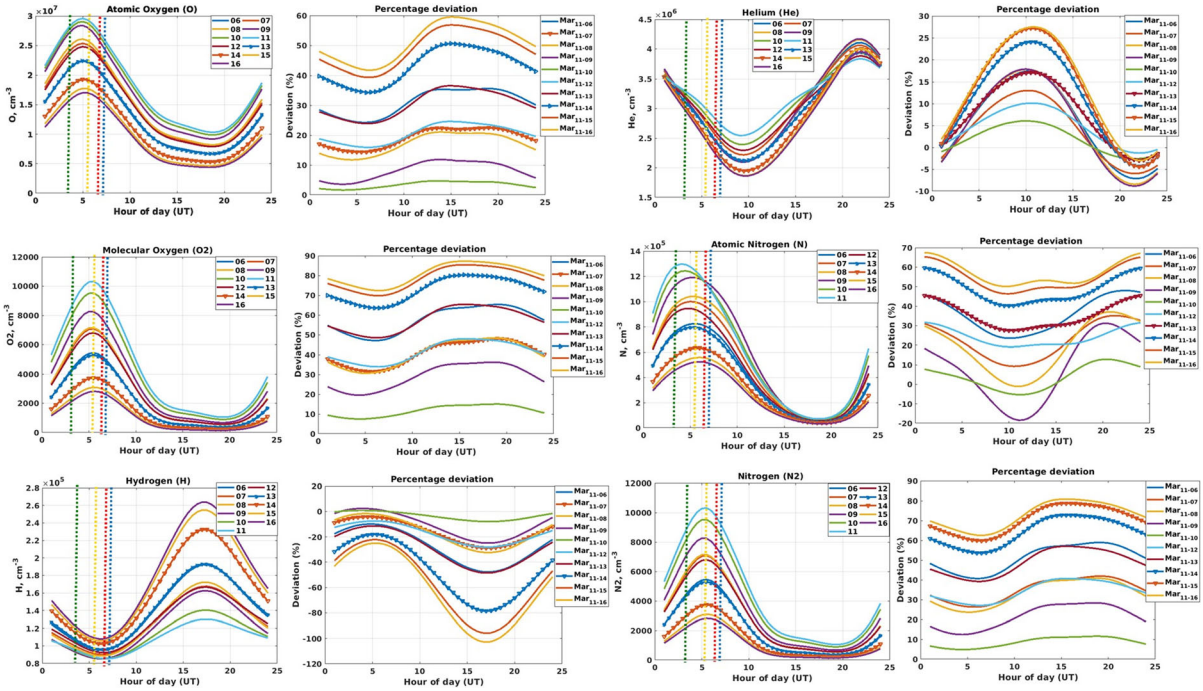

Figure 1

Anomalies of the atmospheric parameters of atomic oxygen (O), oxygen (O2), hydrogen (H), helium (He), atomic nitrogen (N) and nitrogen (N2) with percentage deviation (right side of each parameter) of five days before and after the main earthquake shock on March 11, 2011. The vertical line on each atmospheric parameter indicates the times of significant earthquakes, the green line indicates major foreshock activity on March 09, 2011 at 02:45:20 UT with magnitude M7.3 and depth 32 km; the yellow line indicates the major earthquakes on March 11, 2011 at 05:46:24 UT with magnitude M9.0 and depth 29 km; the red line indicates the aftershocks on March 11, 2011 at 06:15:40 UT with magnitude M7.9 and depth 42.6 km) and the blue line on March 11, 2011 at 06:25:50 UT with magnitude M7.7 and depth 18.6 km

and its lowest value of 752 at 18:50 UT on March 16, 2011. This could be because several authors have suggested that the earthquake preparation process can generate variations in temperature that can affect the energy released in the earthquake (Qin et al., 2021). There could be a fascinating link between radon emissions and thermal anomalies. The most current investigations of earthquake precursors share the assumption of multi-parameter coupling mechanisms (Conti et al., 2021; Picozza et al., 2021; Qin et al., 2021; Tronin, 2006). The total mass density (ρ) value on March 11, 2011 (earthquake day) shows the highest values of all before and after days of the main earthquake day, with 8.637E-16 at 5:00 UT and the lowest value of 1.399E-16 at 18:00 UT on March 16, 2011. The value decreases after the earthquake day, and the percentage deviation of each day is shown in Fig. 2 and Table 2. Unlike the other atmospheric parameters, anomalous oxygen (AO) shows constant variation through all hours of the day. The AO shows a high value of anomalous on the main earthquake day, with a percentage deviation as indicated in Fig. 2 and Table 2. The highest and lowest values of the AO are 1.371E + 04 on March 11, 2011 and 5.413E + 03 on March 15, 2011, respectively. Generally, from Figs. 1 and 2 and Table 2, the average daily and hourly percentage deviation values of the atmospheric parameters for the days of March 06, 07, 08, 09, 10, 12, 13, 14, 15, and 16, 2011 are presented in Tables 1 and 2.

Figure 3a shows this relation of earthquake with the disturbance index ap value and the solar activity variations, which are also indicators of the atmospheric behavior on each day before and after the major earthquake on March 11, 2011. It has recently been established that large earthquakes and the energy produced by the world's seismic activity are influenced by solar activity and the ensuing space

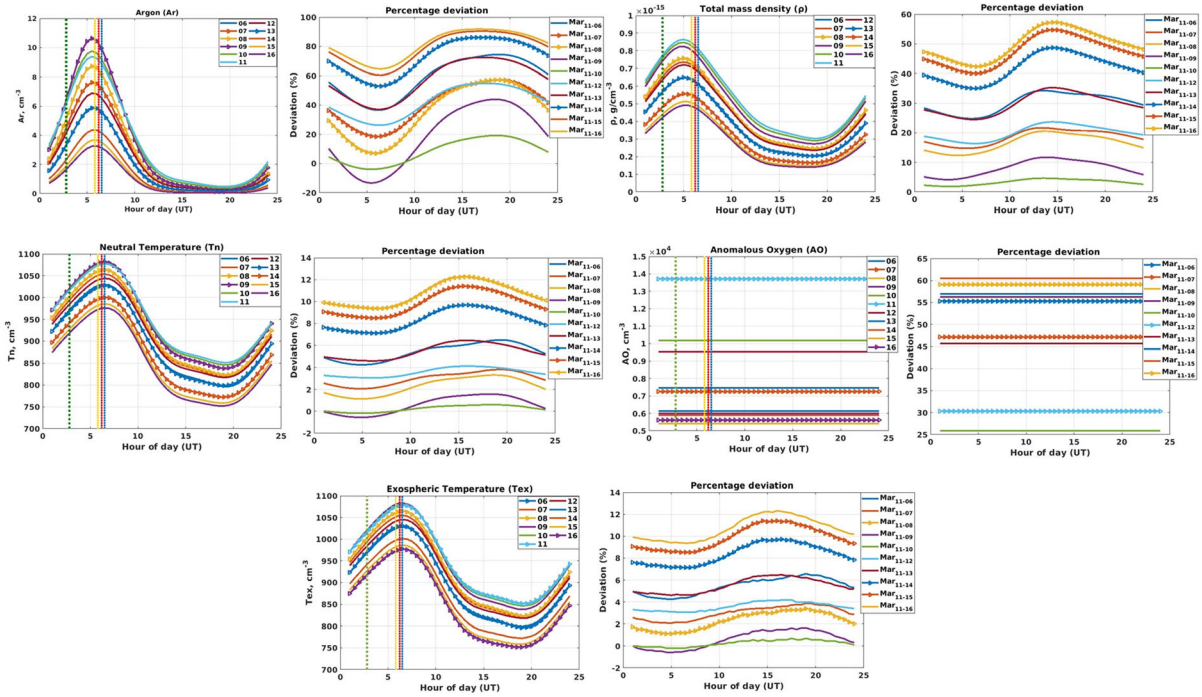

Figure 2

Values of the atmospheric parameters of argon (Ar), total mass density (ρ), neutral temperature (T_n), exospheric temperature (T_{ex}) and anomalous oxygen (AO) with percentage deviation (right side of each parameter) of five days before and after the main earthquake shock on March 11, 2011. The vertical lines on each atmospheric parameter indicate the times of significant earthquakes: the green line (on March 09, 2011 at 02:45:20 UT with magnitude M7.3 and depth 32 km); the yellow line (on March 11, 2011 at 05:46:24 UT with magnitude M9.0 and depth 29 km); the red line (on March 11, 2011 at 06:15:40 UT with magnitude M7.9 and depth 42.6 km) and the blue line (on March 11, 2011 at 06:25:50 UT with magnitude M7.7 and depth 18.6 km)

weather (Anagnostopoulos, 2021). The comparison of the atmospheric parameter values of the five days before and after the major earthquake on March 11, 2011 with the same position (the major earthquake epicenter), year (2011) and time (05:46:24 UT). The atmospheric parameters of atomic oxygen (O), atomic nitrogen (N), helium (He), molecular oxygen (O2), molecular nitrogen (N2), total mass density (ρ), neutral temperature (Tn), exospheric temperature (Tex) and anomalous oxygen (AO) had their highest values during the major earthquake on March 11, 2011. On the other hand, the hydrogen atom has the lowest value on the major earthquake day of March 11, 2011, and the highest value on the non-earthquake day of March 16, 2011. Argon (Ar) had the highest value on the major foreshock activity day of March 09, 2011. This may be due to the chemical potential of the atmosphere for monitoring atmospheric abnormalities before powerful earthquakes caused by a series of processes starting with air ionization brought on by radon radiation from the Earth's crust. Because the last step of radon release before the main shock is modified, atmospheric chemical potential anomalies are produced. Initiating the thermodynamic instability is the ionization of the near-ground layer of the atmosphere by radon, which results in the release of latent heat and changes to the meteorological parameters (air temperature, relative humidity, and air pressure) (Pulinets et al., 2018; Pulinets & Budnikov, 2022). Figure 4 shows that the comparison of the atmospheric parameter values of the five years before the major earthquake on March 11, 2011 with the same position (the major earthquake epicenter), day of the year (March 11) and time (05:46:24 UT), which is a significant earthquake, was not present. The values of most atmospheric parameters during the major earthquake on March 11, 2011, were higher than on non-earthquake days. On the

Table 1

The mean daily percentage deviation values of atmospheric parameter anomalies with respect to the main earthquake shock on March 11, 2011, which are calculated from the diurnal values of percentage deviation of each day

Atmospheric parameters	March 06	March 07	March 08	**March 09**	March 10	***March 11***	March 12	March 13	March 14	March 15	March 16
Atomic oxygen (O)	30.9	19.0	17.0	**8.2**	3.4	***0.0***	20.5	30.5	42.9	48.6	51.1
Oxygen (O_2)	57.5	40.6	40.5	**29.0**	11.7	***0.0***	41.5	57.6	72.8	78.5	80.6
Hydrogen (H)	− 28.1	− 16.1	− 16.4	**− 10.7**	− 3.4	***0.0***	− 17.6	− 29.4	− 47.1	− 57.2	− 62.1
Helium (He)	5.5	3.8	5.2	**5.1**	1.8	***0.0***	4.6	7.5	10.7	12.5	13.4
Atomic nitrogen (N)	35.7	22.3	18.8	**7.4**	3.7	***0.0***	24.1	35.1	48.4	54.3	56.9
Nitrogen (N_2)	51.1	35.0	33.3	**21.5**	8.6	***0.0***	34.4	48.8	64.1	70.2	72.7
Argon (Ar)	58.6	40.3	35.3	**18.4**	8.3	***0.0***	42.2	57.3	72.7	78.5	82.1
Total mass density (ρ)	30.1	18.5	16.6	**8.1**	3.3	***0.0***	20.0	29.8	41.8	47.3	49.7
Neutral temperature (T_n)	5.4	3.0	2.3	**0.6**	0.2	***0.0***	3.6	5.5	8.3	9.8	10.7
Exo. temperature (T_{ex})	5.4	3.0	2.3	**0.6**	0.3	***0.0***	3.6	5.5	8.4	9.9	10.7
Anomalous oxygen (AO)	53.3	47.2	56.2	**56.3**	25.8	***0.0***	30.4	45.7	57.0	60.5	59.1

other hand, the hydrogen atom has the lowest value on the major earthquake day of March 11, 2011, and the highest value on the non-earthquake day of March 11, 2009 (Inchin et al., 2021).

4. Discussion

The Pacific plate and the Okhotsk plate met at Tohoku to produce the great Tohoku earthquake (Ozawa et al., 2011; Hirose et al., 2011; Hayes et al., 2017). A temporal change in the stress field and an increase in the wave amplitude of the seismic reflection properties that point landward indicate the existence of higher pore-fluid pressure in the megathrust zone (Sano et al., 2014). Precursors of the earthquake are generally found in three different sources: surface precursors (land and sea surface temperature), atmospheric precursors (air temperature, relative humidity, outgoing long-wave radiation), and ionospheric precursors (electron densities, electric field disturbances, and high energy particle flux). Mostly, the atmospheric precursors are responsible for the atmospheric parameter anomalies. An earthquake happens when the lithosphere suddenly releases energy. This significant quantity of energy may be released into the atmosphere in the form of acoustic gravity waves and Rayleigh waves that can travel through the atmosphere and into the ionosphere, where they cause changes in the ionosphere and create an extra electric field in the atmosphere. By means of ion-neutral collisions, the energetic particles transported by solar winds settle into the upper thermosphere across the open field lines during the exchange of energy between the geomagnetic field and solar winds. This results in changes to the neutral temperature and electric field (Haider et al., 2024; Heki, 2024), which make the atmospheric parameters anomalies. The seismic reflection in the geological and geophysical interpretation estimates the subsurface acoustic impedance at high and low frequencies (Muhsan et al., 2024). Different reports have been discussed regarding the great 2011 Tohohu earthquake precursors of anomalies: Seismicity (Nagao et al., 2014), pre-seismic land movement (Chen et al., 2013b; Kamiyama et al., 2014), electromagnetic phenomena on the lithosphere (Kopytenko et al., 2011; Xu et al., 2013) and on the atmosphere (Hayakawa, 2018; Ohta et al., 2013), which are the major responsible for the atmospheric parameter anomalies. The results revealed that all of the included atmospheric parameters had contemporary anomalies, as shown in Table 1 and Figs. 1, 2, 3, and 4. The earthquake precursors, such as groundwater level changes, seismicity, surface deformation, temperature change, electric and magnetic fields, and gas emissions, are credible scientific evidence for anomalies in the

Table 2

The hourly percentage deviation values of atmospheric parameter anomalies with respect to the main earthquake shock on March 11, 2011, which are calculated from the hourly values of percentage deviation from minimum values to maximum values of each day

Atmospheric parameters	March 06	March 07	March 08	***March 09***	March 10	***March 11***	March 12	March 13	March 14	March 15	March 16
	Min- Max	Min- Max	Min–Max	***Min–Max***	Min–Max	***Min–Max***	Min–Max	Min–Max	Min–Max	Min–Max	Min–Max
Atomic oxygen (O)	24.3 to 35.7	14.3 to 22.4	11.7 to 21.9	***3.5 to 11.8***	1.6 to 4.7	***0.0***	15.9 to 24.6	23.9 to 36.6	34.4 to 50.6	39.4 to 56.9	41.7 to 59.5
Oxygen (O_2)	47.0 to 65.3	31.4 to 47.9	30.6 to 48.4	***19.5 to 36.2***	7.4 to 15.1	***0.0***	33.9 to 47.9	48.5 to 65.4	63.5 to 80.2	69.7 to 85.5	72.3 to 87.2
Hydrogen (H)	− 47.7 to − 9.9	− 28.8 to − 4.3	− 32.4 to − 1.7	***− 24.9 to 2.5***	− 7.9 to 0.9	***0.0***	− 28.1 to − 7.5	− 48.5 to − 11.4	− 78.6 to 18.2	− 95.9to 22.3	− 102.8 to − 25.0
Helium (He)	− 7.1 to 17.4	− 6.0 to 13.0	− 8.4 to 17.8	***− 8.9 to 17.9***	− 2.6 to 6.1	***0.0***	− 1.3 to 10.1	− 3.0 to 17.1	− 4.4 to 24.0	− 4.5 to 27.1	− 3.0 to 27.5
Atomic nitrogen (N)	23.5 to 48.0	9.2 to 35.1	− 1.1 to 37.0	***− 18.4 to 31.2***	− 5.3 to 12.9	***0.0***	19.1 to 31.6	27.4 to 45.2	40.1 to 59.5	46.3 to 65.3	50.1 to 67.5
Nitrogen (N_2)	40.7 to 58.9	26.3 to 41.9	23.7 to 40.9	***12.4 to 28.4***	4.9 to 11.6	***0.0***	27.1 to 40.7	39.2 to 57.0	53.6 to 72.7	59.8 to 78.7	62.5 to 80.9
Argon (Ar)	36.6 to 74.5	18.5 to 57.2	4.0 to 57.3	***− 13.4 to 43.9***	− 4.0 to 19.2	***0.0***	26.2 to 54.9	37.7 to 72.5	53.0 to 86.2	60.4 to 90.4	64.6 to 91.8
Total mass density (ρ)	42.3 to 57.3	14.7 to 21.7	12.3 to 20.6	***4.1− 11.7***	1.8− 4.6	***0.0***	16.3 to 23.7	24.5 to 35.3	35.0−48.7	40.0 to 54.7	42.3 to 57.3
Neutral temperature (T_n)	4.3− 6.5	2.1− 3.8	1.1 to 3.3	***− 0.6 to 3.1***	− 0.2 to 0.6	***0.0***	1.1−4.1	4.6−6.4	7.1−9.7	8.5 to 11.4	9.4 to 12.3
Exo. temperature (T_{ex})	4.2 to 6.6	2.1 to 3.9	1.1 to 3.4	***− 0.6 to 1.6***	− 0.2 to 0.7	***0.0***	3.1 to 4.2	4.6 to 6.5	7.1 to 9.7	8.5 to 11.4	9.4 to 12.3
Anomalous oxygen (AO)	53.3	47.2	56.2	***56.3***	25.8	***0.0***	30.4	45.7	57.0	60.5	59.1

Min Minimum percentage deviation value, *Max* Maximum percentage deviation value, *March 09* major foreshock, *March 11* mega main shock of the earthquake

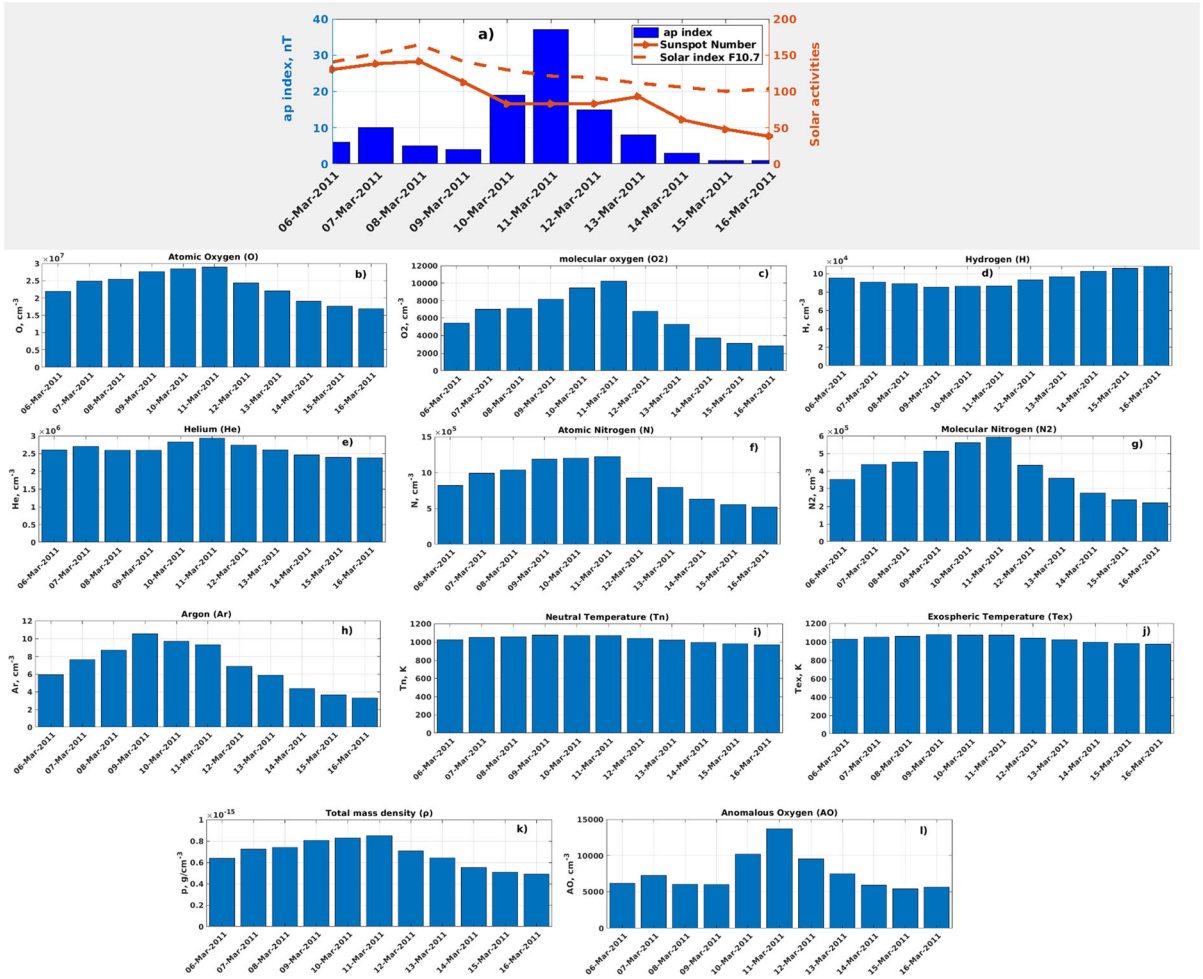

Figure 3
Variation values of the daily ap index and solar activities (**a**) and anomalies of the atmospheric parameters from March 06 to March 16, 2011 (**b-l**) at 05:46:24 UT, five days before and after the main earthquake shock with magnitude M 9.0 on March 11, 2011

atmospheric parameters (Cicerone et al., 2009). On the other hand, lithospheric variations (Lin et al., 2023); the ultra-low-frequency magnetic field emissions associated with the earthquake (Han et al., 2011, 2015; Xu et al., 2013; Swati et al., 2020; Zhou et al., 2021; Anagnostopoulos, 2021); the waveforms of underground currents increasing due to earthquakes (Simpson, 2008); atmospheric gravity waves (Swati et al., 2020); atmospheric chemical potential (Oikonomou et al., 2021); and atmospheric pressure (Sano et al., 2014; Carpinteri et al., 2019; Inchin et al., 2021) result in both positive and negative atmospheric parameters during the main earthquake shock on March 11, 2011. Orihara et al. (2014) presented the anomalies of groundwater change and temperature level on the M 9.0 Pacific Coast of the Tohoku Earthquake. They observed the anomalies in parameters before the main shock of the Tohoku earthquake on March 11, 2011, which is equivalent to the result obtained in this study.

As shown in Figs. 1 and 2, there are clear diurnal variations between the main earthquake day and non-earthquake days. As indicated in the study by Reber et al. (1973), atmospheric parameters show different densities peaking hours around an altitude of 450 km. Other parameters, such as hydrogen (which has peak values around 18:00 UT), helium (which has peak values around 22:00 UT), and anomalous oxygen

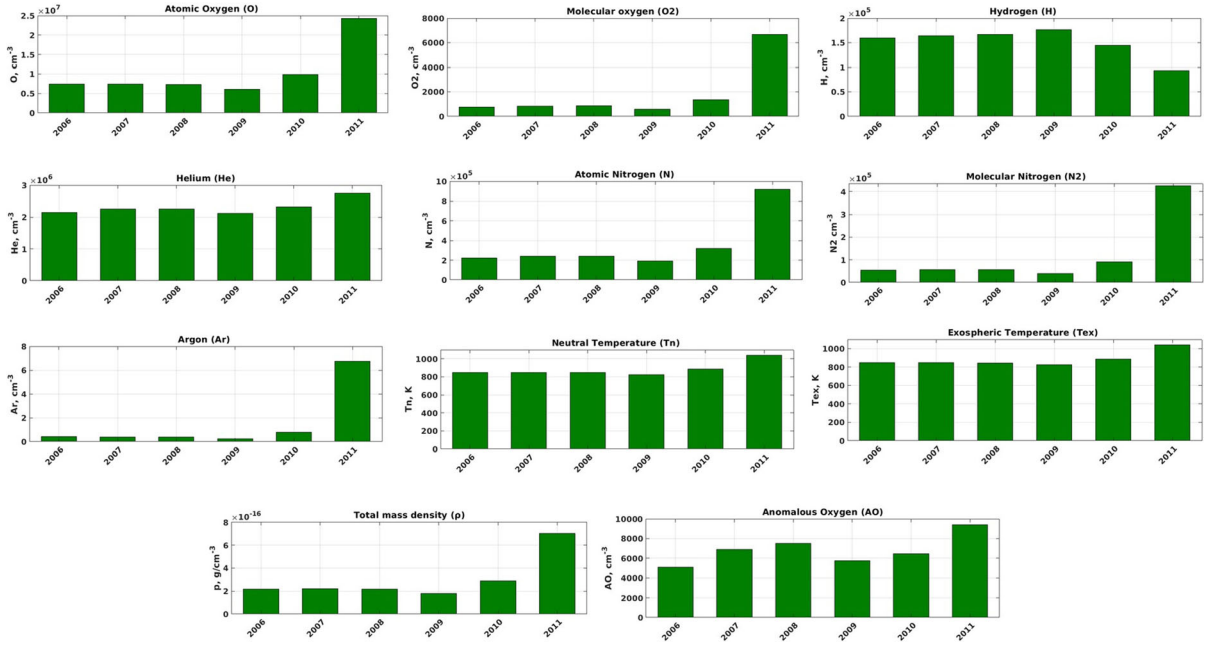

Figure 4
Variation values of the atmospheric parameters and comparison of the values of the 5 years before the major earthquake on March 11, 2011 with the same position (the major earthquake epicenter), day of the year (March 11) and time (05:46:24 UT) without a significant earthquake

(which has a constant value through a day), show their peak values around 5:00 UT during the diurnal variations each day. Except for hydrogen (H), all atmospheric parameters increased during the March 11, 2011 earthquake. Hydrogen (H) decreases during the earthquake day on March 11, 2011 rather than the days before (March 06, 07, 08, 09 and 10) and after (12, 13, 14, 15 and 16). This is probably due to the strong linkages (covalent bonds) with the increased elements of oxygen, helium, nitrogen and others to release energy in the processes (Bar-Nun et al. 1985; Gomis et al., 2004a, 2004b; Mavroyannis & Winicler, 1962). The release of energy during the earthquake is supported by the work of Draz et al. (2021), who analyzed the possibility of precursors from the 2021 Mw 7.1 Japan earthquake from the land surface to the ionosphere and found anomalies as a result of the massive energy release that occurred during the main shock days and the outflow of this seismic energy into the atmosphere. And also, there is a reaction mechanism between hydrogen and oxygen, both in their atomic and molecular forms (Clyne & Thrush, ; Gomis et al., 2004a). On the other hand, there is a reaction mechanism between hydrogen and active nitrogen (Mavroyannis & Winicler, 1962). The atomic oxygen caused chemical reactions in the Earth's mesosphere and lower thermosphere regions. This may be one of the causes of the reduction of atomic hydrogen during the earthquake on March 11, 2011 (Mlynczak & Solomon, 1993; Mlynczak et al. 2013). As shown in Fig. 1, hydrogen and helium in general show similar trends in the hourly variability of their values. This trend may be due to the fact that both helium and hydrogen have similar sizes and are absorbed by other atmospheric parameters and different agents, as reported by different researchers: Kidnay and Hiza (1967); Paine and Seidel (1994); Calvo (2012); Shin and Kwon (2012); and Calvo and Yurtsever (2016). But during the main earthquake shock on March 11, 2011, the helium had higher values than in the five days before and after the major earthquake shock, especially before 18:00 UT. It is generally known that helium may spread more quickly and widely than heat near the main earthquake shock (Sano et al., 1984, 2014).

Most atmospheric parameters show increments during the pre-earthquake period five days before and decreases after the main earthquake shock on March 11, 2011. This is because, as Wallace and Hobbs (2006), Huang et al. (2017) and Wang and Hocke (2022) show, there are strong fundamental linkages between the nature of the precursor and the EQ event. And the anomalies of the atmospheric parameters are due to this linkage, mainly the temperature profile, relative humidity, radio refractivity and infrared emissions, just a few days prior to the event and their repercussions in the low atmospheric profile (Pulinets & Boyarchuk 2004; Pulinets et al., 2006; Huang et al., 2017; Mukherjee & Nandi 2020). In order to comprehend the atmospheric phenomena associated with the main shock, air temperature is used to demonstrate the reaction of seismic activity in the atmosphere with atmospheric parameters (Draz et al., 2021; Heki, 2024). The ratio of the air's vapor pressure to its saturation vapor pressure is commonly referred to as atmospheric relative humidity. Since the atmospheric relative humidity is a function of moisture content and temperature, its variability is dependent on the temperature variability, partial pressure of water vapor, and total water-holding capabilities (North et al., 2014). Humidity affects surface fluxes, soil moisture, and the planetary radiative balance both directly and indirectly through cloud formation. The global energy exchange, atmospheric dynamics, earthquake-related atmospheric reaction, and troposphere-stratosphere interaction around the epicenter are also primarily related to the relative humidity status (Heki, 2024). It is also necessary for the development of disturbed weather (Sherwood et al., 2010). Another important linkage among atmospheric parameter anomalies is radio refractivity, which is the bending of radio signals. Radio-refractivity has correlations mostly with atmospheric relative humidity and other atmospheric parameters like atmospheric temperature, atmospheric pressure, and atmospheric water vapor content (Abimbola et al., 2021; Agbo et al., 2021). The refractivity categorization of anomalous propagation situations makes use of the gradient of changed atmospheric refractivity with altitude. The impact of the atmosphere causes undesirable effects when electromagnetic waves propagate through it. The variability of atmospheric refractivity depends on the atmospheric temperature variability in the atmosphere (Emmanuel et al., 2017). Temperature, pressure, and relative humidity are the independent factors that affect radio-refractivity, and they have a direct relationship with the variation in refractivity (Cheloni et al., 2024). Additionally, infrared emission may also have an impact on atmospheric parameter anomalies. This could be attributed to the Earth warming, as some of the incoming solar radiation is absorbed by the surface and atmosphere, and the Earth emits this infrared radiation in the form of heat. The infrared radiation is emitted by clouds, carbon dioxide, and air molecules in the atmosphere, and this mechanism makes the atmospheric parameters anomalies (Smirnov, 2017).

Another important parameter is that the strong gravity waves that are associated with EQ events disrupt the troposphere's normal temperature profile. These gravity waves have a propensity to ascend in the lower atmosphere, which results in an unanticipated deviation in the lower tropospheric temperature profile. This change in temperature could be a sign of a coming EQ event. The temperature rise on the ground surface is immediately noticeable as radon gas is released from underground and this finally leads to atmospheric parameter anomalies. It is important to remember that variations in the tropospheric temperature profile can result from a variety of sources, including convection, meteorological fronts, and instability of jet streams in the troposphere, in addition to gravity waves caused by the underground release of radon gas. Meteorological fronts are a boundary of between two air masses, where warm air in one side and the cold air on the other side. As warm air meets colder air across a front, during this a significant atmospheric temperature changes may occur. On the other hand the strong jet streams are typically found in upper level fronts and makes this the air surface disturbances. Seismicity creates an environment in which large-scale electric charge separation occurs in the crust of the earth during earthquake development. As the electron temperature rises, so does the atmospheric temperature (Alimov et al., 1989). This may also lead to the atmospheric parameter anomalies. Measurements of temperature, composition, and winds in the neutral

atmosphere are essential to answering many scientific issues. Temperature is the most significant atmospheric parameter that influences the radon concentration both directly and indirectly by altering the lithosphere air flows. There is the highest and most direct correlation between the radon concentration and the external temperature (Pinault et al., 1996; Garavaglia et al., 2000). Numerous seismo-related parameters, including electromagnetic field, temperature fluctuation, exhalation of gases and aerosols, and lithospheric deformation, may be observed from space to ground (Conti et al., 2021; Picozza et al., 2021) during the earthquake. But different scholars agree that the earthquake preparation process stage could generate temperature variability that may be caused by the flow or exhalation of geochemical fluids on the deep lithosphere, and temperature variability may have an impact on the energy budget in the lithosphere-atmosphere–ionosphere coupling system of the sequences of the earthquake (Conti et al., 2021; Picozza et al., 2021; Qin et al., 2021, and references therein).

The molecular oxygen (O2) and molecular nitrogen (N2) also showed high values during the earthquake on March 09, 2011, as shown in Fig. 1. Reactive trace gases like nitrogen oxides can transform into different chemical species like fine particle matter and ozone (Rey-Pommier et al., 2023) to increase the reaction mechanisms in the atmospheric parameters. This may be due to the March 11, 2011 earthquake that generated acoustic waves and disrupted atmospheric pressure, which resulted in concentrations of N2 and O2 oxidation (Carpinteri & Niccolini, 2019; Fikeraddis & Endeshaw, 2020; Oikonomou et al., 2021; Lin et al., 2023). Additionally, this could be because, as stated by Pulinets et al. (2015), gaseous radon produces huge hydrated ion clusters that result in the formation of preseismic thermal anomalies before an earthquake due to latent heat emission as well as preseismic atmospheric abnormalities. The only radioactive gas that may travel underground from the earth's surface to its surface origin, uranium, is radon, which is naturally occurring and is released into the atmosphere (Pulinets et al., 2022). The total mass density (ρ), neutral temperature (Tn) and exospheric temperature (Tex) as shown in Fig. 2, had high values during the earthquake starting on March 09, 2011. This is due to the fact that several authors have suggested that the earthquake preparation process can generate variations in temperature that can affect the energy released in the earthquake (Qin et al., 2021). There could be a fascinating link between radon emissions and thermal anomalies. The most current investigations of earthquake precursors share the assumption of multi-parameter coupling mechanisms (Conti et al., 2021; Picozza et al., 2021; Qin et al., 2021; Tronin, 2006). Since the atmospheric temperature is a measure of the average speed of all molecules in the atmosphere, the earthquake-generated acoustic waves and the earth's pressure warm the surface of the entire atmosphere, resulting in a disturbance of the density of electrons in the atmosphere. The related work by Liu et al. (2023b) analyzed the oxygen ion density and the vertical ion drift velocity under earthquake condition and foundings show that the increase in oxygen ion density, electron density and electron temperature within 1 to 15 days before strong earthquake. The combination of gases that envelops the Earth has been referred to as the atmosphere. This mass of air contributes to the possibility of life by giving us air to breathe, protecting us from the sun's damaging ultraviolet radiation, retaining heat to warm the planet, and reducing drastic temperature swings between night and day. On the other hand, our environment's most vulnerable geophysical shell is the atmosphere. The chemical potential of the atmosphere for monitoring anomalies in the atmosphere before powerful earthquakes caused by a series of processes started by air ionization brought on by radon emissions from the Earth's crust. Forecasting for the short term using atmospheric chemical potential is possible in the event of earthquakes and volcano eruptions (Pulinets & Budnikov, 2022). Based on the temperature variability, the atmosphere can be divided into the troposphere, stratosphere, mesosphere, thermosphere, and exosphere (a further area that starts around 500 km above the surface of the Earth). All these regions of the atmosphere may be affected by the sequence of the earthquake. The Earth's atmosphere is deposited with energy by energetic particles from space, which also affect changes in the concentration of neutral components like ozone, which regulates the balance of

atmospheric temperature and also affects the variability of other atmospheric compositions. The ionization of the atmosphere is one of the most interesting mechanisms for establishing a link between space weather events and the terrestrial environment (Murase et al., 2023). Gravity waves, which develop in different fluids, are balanced by buoyancy and gravity forces. This atmospheric gravity wave may be seen in the Earth's atmosphere at different altitudes, extending from the troposphere into the thermosphere (Gunzkofer et al., 2023; Horváth et al., 2024). The occurrence and propagation of the traveling ionization disturbances are primarily effects of acoustic and gravitational waves on the thermosphere. One of the major causes of atmospheric gravity waves is earthquakes. This wave can also affect the overall thermospheric circulations (Zawdie et al., 2022) and be responsible for anomalies in the atmospheric parameters. Generally, in this study on the atmospheric parameters, there were anomalies observed with positive and negative percentage deviations, which is in agreement with the studies presented by Liu et al. (2004), Shah et al. (2020b), Oikonomou et al. (2021) and Lin et al. (2023).

At the time of the Tohoku earthquake, solar activity and geomagnetic activity were also much disturbed (Le et al., 2013). To validate this explanation, it is necessary to determine to what extent solar activity and geomagnetic activity can cause atmospheric anomalies in the atmosphere. Seismicity creates an environment in which large-scale electric charge separation occurs in the crust of the earth during earthquake development. As the electron temperature rises, so does the atmospheric temperature (Alimov et al., 1989). This may also lead to whole atmospheric parameter anomalies. On the other hand, during the major shock day, when geomagnetic activity remained quiet, Shah et al. (2020a) detected abnormalities in atmospheric and ionospheric parameters within the seismologic zone. Even if additional investigation is needed in this regard, the observed anomalies are due to the earthquake or the geomagnetic storm during the Tohoku earthquake. A detailed analysis by Le et al. (2013) of the ionospheric anomalies was presented three days before the 9.0-magnitude Tohoku earthquake on March 11, 2011. They concluded that the solar and geomagnetic activities were not enough to cause the observed ionospheric increases for a long time, and these regional anomalies might be related to the greatest earthquake in Tohoku. Additionally, Le et al. (2011) used GPS TEC data to study statistically the pre-earthquake ionospheric anomaly for a total of 736 earthquakes with a magnitude higher or equal to 6 from 2002 to 2010. The results of their study suggest that the prevalence of anomalies within several days before the earthquakes is higher than during the background days, particularly for larger magnitude and low-depth earthquakes. This conclusion implies that there may also be atmospheric anomalies; although earthquakes originate in the lithosphere, they can also interact with the lower atmosphere and ionosphere, and following that, the Lithosphere-Atmosphere–Ionosphere Coupling Mechanism of the Great Tohoku Earthquake on March 11, 2011.

To conclude, the atmospheric anomalies observed on the model measurement imply that, in addition to the Tohoku earthquake, these anomalies may be related to the solar and geomagnetic activities during the period (Le et al., 2013). In this scenario, satellite observations of the atmosphere play an important role in determining the possibility of detecting abnormalities in atmospheric parameters as short-lived precursors of earthquakes (Pulinets et al., 2006; Sharzehei et al., 2015). Some authors used this empirical model for the investigation of atmospheric anomalies during the Great Tohoku Earthquake on March 11, 2011 and other earthquakes. For example: The study by Kakinami et al. (2021) calculated the vertical profile of neutral temperature given by the NRLMSISE-00 model during the Great Tohoku earthquake. Arai et al. (2011) observed certain atmospheric parameter abnormalities in their investigation of the 9.0-magnitude Tohoku earthquake on March 11, 2011. According to Freund et al. (2022), atmospheric parameter anomalies during earthquakes are caused by the lithosphere-atmosphere coupling mechanism. The study identifies an expected relationship between atmospheric processes and subsequent earthquakes ($M > 6$) throughout a large region of Japan. However, doubts exist about how the NRLMSISE-00 model is adapted to assess seismic disturbances in the atmosphere. An empirical model,

also known as a statistical model, is based on observation rather than theory (Liu et al., 2023a). So the ability of the NRLMSISE-00 model to capture the atmospheric parameter anomalies during the period of the earthquake may be due to the considerable number of real observations for atmospheric parameter measurement. In the future, this issue will be analyzed in detail with the help of additional observations in another work.

5. Conclusion

The shaking of the Earth's surface due to the passage of seismic waves in the Earth's outermost layer is known as an earthquake and the tectonic plates bordering the earth are where the majority of earthquakes occur (Nagamatsu et al., 2011; Pulinets et al., 2015; Chandrappa & Umesh, 2016; Manisalidis et al., 2020; Fawzy et al., 2020). Numerous factors, such as the emission of latent heat of evaporation during the condensation of water vapor, temperature of groundwater chemistry, changes in the rock's magnetic and electric fields, the thermal anomalies near the Earth's surface, the emission of radon and other ionized gases, the electromagnetic fluctuations at various frequencies, the horizontal gradients of the temperature and pressure triggered, the formation of the linear cloud structures, the energetic electrons radiation belts and the precipitation, atmospheric conductivity and atmospheric gravity wave leading to the anomalies in the atmospheric parameters (Hayakawa, 2018; Oyama et al., 2019; Pulinets et al., 2015, 2022; Woith, 2015). The precursory nature of radon variations before earthquakes plays a crucial role in the lithosphere-atmosphere mechanism coupling and as do geoelectric, electromagnetic emission, apparent, geodetic, gravity, ground fluid and earthquake hydrology precursors. The most reliable seems to be the atmospheric gravity wave (Pulinets, 2011; Yang et al. 2019b). So one can conclude that a multi-parameter precursor approach provides anomalies in the atmospheric parameters during the study of different earthquake behaviors (Yang et al. 2019b). In this study, the anomalies of the atmosphere are studied by using one of the atmospheric models of the NRLMSISE-00 model data to analyze the atmospheric anomalies of the Tohoku Earthquake on March 11, 2011. In conclusion, the findings, which are shown in Figs. 1, 2, 3, and 4 and Tables 1 and 2, confirm the existence of contemporary anomalies in all of the included atmospheric parameters. Except for hydrogen (H), all atmospheric parameters increased during the March 11, 2011 earthquake. Hydrogen (H) decreases during the earthquake day on March 11, 2011 rather than the days before and after. The Tohoku Earthquake atmospheric parameter anomalies are well captured by the NRLMSISE-00 model. The NRLMSISE-00 model's ability to capture atmospheric parameter anomalies during the earthquake may be due to the enormous number of real observations for atmospheric parameter measurement.

Acknowledgements

The author gratefully acknowledge the NRLMSISE-00 model developer and freely access online on website: https://ccmc.gsfc.nasa.gov/modelweb/models/nrlmsise00.php.

Author contributions All works submitted for publication, including study conception and design, material preparation, data collection and analysis, draft and final manuscript writing, were performed by Lake Endeshaw.

Funding

No funding was received for conducting this study. The author has no relevant financial or non-financial interests to disclose.

Data availability

The data sets generated during the current study are freely available to any researcher wishing to use them for non-commercial purposes on the following website: https://ccmc.gsfc.nasa.gov/modelweb/models/nrlmsise00.php.

Declarations

Competing interests The author declares no competing interests.

Conflict interests The author declares that he has no known competing financial interests or personal relationships that could have appeared to influence the work reported in this paper.

References

Abimbola, O. J., Bada, S. O., Falaiye, A. O., Sukam, Y. M., Otto, M. S., & Muhammad, S. (2021). Estimation of radio refractivity from satellite-derived meteorological data over a decade for West Africa. *Scientific African, 14*, e01054. https://doi.org/10.1016/j.sciaf.2021.e01054

Afraimovich, E. L., Astafieva, E. I., & Kirushkin, V. (2006). Localization of the source of ionospheric disturbance generated during an earthquake. *International Journal of Geomagnetism and Aeronomy, 6*, 1–13. https://doi.org/10.1029/2004GI000092

Agbo, E. P., Ettah, E. B., & Eno, E. E. (2021). The impacts of meteorological parameters on the seasonal, monthly, and annual variation of radio refractivity. *Indian Journal of Physics, 95*, 195–207. https://doi.org/10.1007/s12648-020-01711-9

Ahmed, J., Shah, M., Awais, M., Jin, S., Zafar, W. A., Ahmad, N., Amin, A., Shah, M. A., & Ali, I. (2022). Seismo-ionospheric anomalies before the 2019 Mirpur earthquake from ionosonde measurements. *Advances in Space Research, 69*, 26–34. https://doi.org/10.1016/j.asr.2021.07.030

Akhoondzadeh, M., & De Santis, A. (2022). Is the apparent correlation between solar-geomagnetic activity and occurrence of powerful earthquakes a casual artifact? *Atmosphere, 13*, 1131. https://doi.org/10.3390/atmos13071131

Alimov, O. A., Gokhberg, M. B., Liperovskaia, E. V., Gufeld, I. L., Liperovsky, V. A., & Roubtsov, L. N. (1989). Anomalous characteristics of the middle latitude Es layer before earthquakes. *Physics of the Earth and Planetary Interiors, 57*(1–2), 76–81. https://doi.org/10.1016/0031-9201(89)90216-1

Al-Taie, A. J., & Albusoda, B. S. (2019). Earthquake hazard on Iraqi soil: Halabjah earthquake as a case study. *Geodesy and Geodynamics, 10*, 196–204.

Anagnostopoulos, G. (2021). On the origin of ULF magnetic waves before the Taiwan Chi–Chi 1999 earthquake. *Frontiers in Earth Science, 9*, 730162. https://doi.org/10.3389/feart.2021.730162

Anagnostopoulos, G., Spyroglou, I., Rigas, A., Preka-Papadema, P., Mavromichalaki, H., & Kiosses, I. (2021). The sun as a significant agent provoking earthquakes. *The European Physical Journal of Special Topics, 230*, 287–333. https://doi.org/10.1140/epjst/e2020-000266-2

Arai N., Iwakuni, M., Watada, S., Imanishi, Y., Murayama, T., & Nogami, M. (2011). Atmospheric boundary waves excited by the tsunami generation related to the 2011 great Tohoku-Oki earthquake. *Geophysical Research Letters, 38*(7) https://doi.org/10.1029/2011GL049146

Astafyeva, E. (2019). Ionospheric detection of natural hazards. *Reviews of Geophysics, 57*, 1265–1288.

Bakhmutov, V. G., Sedova, F. I., & Mozgovaya, T. A. (2007). Geomagnetic disturbances and earthquakes in the Vrancea zone. *Izvestiya Physics of the Solid Earth, 43*, 931–937. https://doi.org/10.1134/S1069351307110031

Bokov, V. N. (2004). Variability of atmospheric circulation—the initiator of strong earthquakes. *Ural'skii Geofizicheskii Vestnik, 6*, 5–11. In Russian.

Bruinsma, S., & Boniface, C. (2021). The operational and research DTM-2020 thermosphere models. *Journal of Space Weather and Space Climate, 11*, 47. https://doi.org/10.1051/swsc/2021032

Calabia, A., Geshi, T., & Shuanggen, J. (2019). Assessment of new thermospheric mass density model using NRLMSISE- 00 model, GRACE, Swarm-C, and APOD observations. *Journal of Atmosphere and Solar Physics, 199*, 105207. https://doi.org/10.1016/j.jastp.2020.105207

Calvo, F. (2012). Size-induced melting and reentrant freezing in fullerene-doped helium clusters. *Physical Review B, 85*, 060502.

Calvo, F., & Yurtsever, E. (2016). Solvation of carbonaceous molecules by para-H2 and ortho-D2 clusters I Polycyclic aromatic hydrocarbons. *The Journal of Chemical Physics, 145*, 084304.

Carpinteri, A., & Niccolini, G. (2019). Correlation between the fluctuations in worldwide seismicity and atmospheric carbon pollution. *Sci, 1*(1), 17. https://doi.org/10.3390/sci1010017

Chandrappa R, CK Umesh (2016) *Environmental Science and Engineering Sustainable Air Pollution Management, Air Pollution and Disasters,* https://doi.org/10.1007/978-3-319-21596-9 *(Chapter 8), 325–343,* https://doi.org/10.1007/978-3-319-21596-9_8

Cheloni, D., Famiglietti, N. A., Tolomei, C., Caputo, R., & Vicari, A. (2024). The 8 September 2023, MW 6.8, Morocco earthquake: A deep transpressive faulting along the active high Atlas mountain belt. *Geophysical Research Letters, 51*, e2023GL106992. https://doi.org/10.1029/2023GL106992

Chen, C. H., Wen, S., Liu, J. Y., Hattori, K., Han, P., Hobara, Y., Wang, C. H., Yeh, T. K., & Yen, H. Y. (2013b). Surface displacements in Japan before the 11 March 2011 M.9.0 TōhokuOki earthquake. *Journal of Asian Earth Sciences, 80*, 165–171.

Chen, H., Wang, R., Miao, M., Liu, X., Ma, Y., Hattori, K., & Han, P. (2020). A statistical study of the correlation between geomagnetic storms and M ≥ 7.0 global earthquakes during

1957–2020. *Entropy, 22*(11), 1270. https://doi.org/10.3390/e22111270

Chen, X., Hu, X., Xiao, C., & Wang, X. (2013a). Correction method of the low earth orbital neutral density prediction based on the satellites data and NRLMSISE-00 model. *Chinese Journal of Geophysics, 56*, 3246–3254.

Cicerone, R. D., Ebel, J. E., & Britton, J. (2009). A systematic compilation of earthquake precursors. *Tectonophysics, 476*(3), 371–396. https://doi.org/10.1016/j.tecto.2009.06.008

Clyne, M., & Thrush, B. (1961). Reaction of oxygen atoms with hydrogen. *Nature, 189*, 135–136. https://doi.org/10.1038/189135a0

Conker, R., El-Arini, M., Albertson, T., Klobuchar, J., & Doherty, P. (1997). Description and assessment of real-time algorithms to estimate the ionospheric error bounds for WAAS. *Journal of Navigation, 44*, 77–87.

Conti, L., Picozza, P., & Sotgiu, A. (2021). A critical review of ground based observations of earthquake precursors. *Frontiers in Earth Science, 9*, 676766. https://doi.org/10.3389/feart.2021.676766

De Santis, A., DeFranceschi, G., & Kerridge, D. (1994). Regional spherical modeling of 2-D functions: The case of the critical frequency of the F2 ionospheric layer. *Computers and Geosciences, 20*, 849–871.

DeMets, C. (1992a). Oblique convergence and deformation along the Kuril and Japan trenches. *Journal of Geophysical Research, 97*, 17615–17625.

DeMets, C. (1992b). A test of present-day plate geometries for northeast Asia and Japan. *Journal of Geophysical Research, 97*, 17627–17635.

Dimitar, O., Sergey, P., Alexey, R., Alexander, R., Konstantin, T., Dmitri, D., et al. (2011). Atmosphere-ionosphere response to the M9 Tohoku earthquake revealed by multi-instrument space-borne and ground observations: Preliminary results. *Earthquake Science, 24*, 1–7. https://doi.org/10.1007/s11589-011-0817-z

Draz, M. U., Shah, M., Jamjareegulgarn, P., Shahzad, R., Hasan, A. M., & Ghamry, N. A. (2023). Deep machine learning based possible atmospheric and ionospheric precursors of the 2021 Mw 7.1 Japan earthquake. *Remote Sensing.*, 15. https://doi.org/10.3390/rs15071904

Emmanuel, I., Adeyemi, B., Ogolo, E. O., & Adediji, A. T. (2017). Characteristics of the anomalous refractive conditions in Nigeria. *Journal of Atmospheric and Solar-Terrestrial Physics, 164*, 215–221. https://doi.org/10.1016/j.jastp.2017.08.023

Emmert, J. T. (2015). Thermospheric mass density: A review. *Advances in Space Research, 56*, 773–824.

Emmert, J. T., Drob, D. P., Picone, J. M., Siskind, D. E., Jones, M., Jr., Mlynczak, M. G., et al. (2020). NRLMSIS 2.0: a whole-atmosphere empirical model of temperature and neutral species densities. *Earth and Space Science, 7*, e2020EA001321. https://doi.org/10.1029/2020EA001321

Emmert, J. T., Jones, M., Jr., Siskind, D. E., Drob, D. P., Picone, J. M., Stevens, M. H., et al. (2022). NRLMSIS 2.1: An empirical model of nitric oxide incorporated into MSIS. *Journal of Geophysical Research: Space Physics, 127*, e2022JA030896. https://doi.org/10.1029/2022JA030896

Fawzy, S., Osman, A. I., Doran, J., et al. (2020). Strategies for mitigation of climate change: A review. *Environmental Chemistry Letters, 18*, 2069–2094. https://doi.org/10.1007/s10311-020-01059-w

Fikeraddis, M., & Endeshaw, L. (2020). Influence of temperature and relative humidity on air pollution in Addis Ababa, Ethiopia. *Journal of Environmental and Earth Sciences., 02*(2), 19–25. https://doi.org/10.30564/jees.v2i2.2286

Freund, F. T., Mansouri Daneshvar, M. R., & Ebrahimi, M. (2022). Atmospheric storm anomalies prior to major earthquakes in the Japan Region. *Sustainability, 14*, 10241. https://doi.org/10.3390/su141610241

Garavaglia, M., Dal Moro, G., & Zadro, M. (2000). Radon and tilt measurements in a seismic area: Temperature effects. *Physics and Chemistry of the Earth, Part a: Solid Earth and Geodesy, 25*(3), 233–237. https://doi.org/10.1016/S1464-1895(00)00038-7

Ghosh, D., Deb, A., & Sengupta, R. (2009). Anomalous radon emission as precursor of earthquake. *Journal of Applied Geophysics, 69*(2), 67–81. https://doi.org/10.1016/j.jappgeo.2009.06.001

Gomis, O., Leto, G., & Strazzulla, G. (2004a). Hydrogen peroxide production by ion irradiation of thin water ice films. *Astronomy & Astrophysics, 420*, 405. https://doi.org/10.1051/0004-6361:20041091

Gomis, O., Satorre, M. A., Strazzulla, G., & Leto, G. (2004b). Hydrogen peroxide formation by ion implantation in water ice and its relevance to the Galilean satellites. *Planetary and Space Science, 52*, 371–378. https://doi.org/10.1016/j.pss.2003.06.010

Guglielmi, A. V., & Klain, B. I. (2020). On the influence of the Sun on the seismicity of the Earth. *Solnechno Terrestrial Physics, 6*(1), 111–115. https://doi.org/10.12737/szf-61202010

Guglielmi, A. V., Klain, B. I., & Kurazhkovskaya, N. A. (2020). Earthquakes and geomagnetic disturbances. *Solnechno Terrestrial Physics, 6*(4), 80–83. https://doi.org/10.12737/szf-64202012

Guglielmi, A. V., Klain, B. I., & Kurazhkovskaya, N. A. (2021). On the correlation of earthquakes with geomagnetic storms. *Izvestiya Physics of the Solid Earth, 57*, 994–998. https://doi.org/10.1134/S1069351321060021

Gunzkofer, F., Pokhotelov, D., Stober, G., Mann, I., Vadas, S. L., Becker, E., Tjulin, A., Kozlovsky, A., Tsutsumi, M., Gulbrandsen, N., Nozawa, S., Lester, M., Belova, E., Kero, J., Mitchell, N. J., & Borries, C. (2023). Inferring neutral winds in the ionospheric transition region from atmospheric-gravity-wave traveling-ionospheric-disturbance (AGW-TID) observations with the EISCAT VHF radar and the Nordic Meteor Radar Cluster. *Annales Geophysicae, 41*, 409–428. https://doi.org/10.5194/angeo-41-409-2023

Haider, S. F., Shah, M., Li, B., de Jamjareegulgarn, P., OliveiraJúnior, J. F., & Zhou, C. (2024). Synchronized and co-located ionospheric and atmospheric anomalies associated with the 2023 Mw 7.8 Turkey earthquake. *Remote Sensing., 16*, 222. https://doi.org/10.3390/rs16020222

Han, P., Hattori, K., Huang, Q., Hirano, T., Ishiguro, Y., Yoshino, C., & Febriani, F. (2011). Evaluation of ULF electromagnetic phenomena associated with the 2000 Izu Islands earthquake swarm by wavelet transform analysis. *Natural Hazards and Earth System Sciences, 11*, 965–970. https://doi.org/10.5194/nhess-11-965-2011

Han, P., Hattori, K., Xu, G., Ashida, R., Chen, C. H., Febriani, F., & Yamaguchi, H. (2015). Further investigations of geomagnetic diurnal variations associated with the 2011 off the Pacific coast of Tohoku earthquake (Mw 9.0). *Journal of Asian Earth Sciences, 114*(2), 321–326. https://doi.org/10.1016/j.jseaes.2015.02.022

Hayakawa, M. (2018). Earthquake precursor studies in Japan. *Pre-Earthquake Processes: A Multidisciplinary Approach to Earthquake Prediction Studies*, 7–18.

Hayakawa, M., & Hobara, Y. (2010). Current status of seismo-electromagnetics for short-term earthquake prediction. *Geomatics Natural Hazards Risk, 1*, 115–155.

Hayes, G.P., Myers, E.K., Dewey, J.W., Briggs, R.W., Earle, P.S., Benz, H.M., Smoczyk, G.M., Flamme, H.E., Barnhart, W.D., Gold, R.D., Furlong, K.P. (2017). Tectonic summaries of magnitude 7 and greater earthquakes from 2000 to 2015: U.S. Geological Survey Open-File Report 2016–1192, pp. 148, https://doi.org/10.3133/ofr20161192.

Hedin, A. E. (1983). A revised thermospheric model on mass spectrometer and incoherent scatter data: MSIS-83. *Journal of Geophysical Research, 88*, 10170–10188.

Hedin, A. E. (1987). MSIS-86 thermospheric model. *Journal of Geophysical Research, 92*, 4649–4662.

Hedin, A. E. (1991). Extension of the MSIS thermosphere model into the middle and lower atmosphere. *Journal of Geophysical Research, 96*, 1159–1172.

Hedin, A. E., Reber, C. A., Newton, G. P., Spencer, N. W., Brinton, H. C., Mayr, H. G., & Potter, W. E. (1977). A global thermospheric model based on mass spectrometer and incoherent scatter data, MSIS 1: N 2 density and temperature. *Journal of Geophysical Research, 82*, 2139–2147.

Heki, K. (2011). Ionospheric electron enhancement preceding the 2011 Tohoku-Oki earthquake. *Geophysical Research Letters, 38*, 17. https://doi.org/10.1029/2011GL047908

Heki, K. (2024). Atmospheric resonant oscillations by the 2022 January 15 eruption of the Hunga-Tonga Hunga-Ha'apai volcano from GNSS-TEC observations. *Geophysical Journal International, 236*, 1840. https://doi.org/10.1093/gji/ggae023

Hirose, F., Miyaoka, K., Hayashimoto, N., et al. (2011). Outline of the 2011 off the Pacific coast of Tohoku Earthquake (Mw 90) Seismicity: foreshocks, mainshock, aftershocks, and induced activity. *Earth Planet and Space, 63*, 513. https://doi.org/10.5047/eps.2011.05.019

Hobara, Y., Watanabe, M., Miyajima, R., Kikuchi, H., Tsuda, T., & Hayakawa, M. (2022). On the spatio-temporal dependence of anomalies in the atmospheric electric field just around the time of earthquakes. *Atmosphere, 13*, 1619. https://doi.org/10.3390/atmos13101619

Horváth, Á., Vadas, S. L., Stephan, C. C., & Buehler, S. A. (2024). One-minute resolution GOES-R observations of Lamb and gravity waves triggered by the Hunga Tonga-hunga Ha'apai eruptions on 15 January 2022. *Journal of Geophysical Research: Atmospheres, 129*, e2023JD039329. https://doi.org/10.1029/2023JD039329

Huang, F., Li, M., Ma, Y., Han, Y., Tian, L., Yan, W., & Li, X. (2017). Studies on earthquake precursors in China: a review for recent 50 years. *Geodesy and Geodynamics, 8*(1), 1–12. https://doi.org/10.1016/j.geog.2016.12.002

Inchin, P. A., Snively, J. B., Kaneko, Y., Zettergren, M. D., & Komjathy, A. (2021). Inferring the evolution of a large earthquake from its acoustic impacts on the ionosphere. *AGU Advances, 2*, e2020AV000260. https://doi.org/10.1029/2020AV000260

Jin, S., Occhipinti, G., & Jin, R. (2015). GNSS ionospheric seismology: Recent observation evidences and characteristics. *Earth Science Reviews, 147*, 54–64.

Junqueira Saldanha, M. H., & Hirata, Y. (2022). Solar activity facilitates daily forecasts of large earthquakes. *Chaos: An Interdisciplinary Journal of Nonlinear Science*, *32*(6), https://doi.org/10.1063/5.0096150

Kakinami, Y., Saito, H., Yamamoto, T., Chen, C.-H., Yamamoto, My., Nakajima, K., et al. (2021). Onset altitudes of co-seismic ionospheric disturbances determined by multiple distributions of GNSS TEC after the foreshock of the 2011 Tohoku Earthquake on March 9, 2011. *Earth and Space Science, 8*, e2020EA001217. https://doi.org/10.1029/2020EA001217

Kamiyama, M., Sugito, M., Kuse, M., Chekotov, A., & Hayakawa, M. (2014). On the precursors to the 2011 Tōhoku earthquake: crustal movements and electromagnetic signatures. *Geomatics, Natural Hazards and Risk.* https://doi.org/10.1080/19475705.2014.937773

Kavanagh, A. J., Cobbett, N., & Kirsch, P. (2018). Radiation belt slot region filling events: sustained energetic precipitation into the mesosphere. *Journal of Geophysical Research Space Physics, 123*(9), 7999–8020. https://doi.org/10.1029/2018JA025890

Khachikyan, G., Inchin, A., & Lozbin, A. (2012). Spatial distribution of seismicity: relationships with geomagnetic Z-component in geocentric solar magnetospheric coordinate system. *International Journal of Geosciences, 3*, 1084–1088.

Khachikyan, G., Stikhamaya, G. G., Stikhamiy, A. P., & Solonitsina, N. F. (2008). Spatial distribution of earthquake epicenters and geomagnetic declination angle. *Inland Earthquake, 22*, 264–270.

Kidnay, A. J., & Hiza, M. J. (1967). High pressure adsorption isotherms of neon, hydrogen, and helium at 76°K. In K. D. Timmerhaus (Ed.), *Advances in cryogenic engineering*. (Vol. 12). Boston: Springer. https://doi.org/10.1007/978-1-4757-0489-1_77

KopytenkoYu, A., Ismaguilov, V. S., Hattori, K., & Hayakawa, M. (2012). Anomaly disturbances of the magnetic fields before the strong earthquake in Japan on March 11, 2011. *Annales Geophysicae., 55*(1), 101–107. https://doi.org/10.4401/ag-5260

Kotov, D., Richards, P. G., Reznychenko, M., Bogomaz, O., et al. (2023). Interhemispheric ionosphere-plasmasphere system shows a high sensitivity to the exospheric neutral hydrogen density: A caution of the global reference atmospheric model hydrogen density. *Frontiers in Astronomy and Space Science., 10*, 1113706. https://doi.org/10.3389/fspas.2023.1113706

Kotov, D. V., Richards, P. G., Truhlík, V., Bogomaz, O. V., Shulha, M. O., Maruyama, N., et al. (2018). Coincident observations by the Kharkiv IS radar and ionosonde, DMSP and Arase (ERG) satellites, and FLIP model simulations: Implications for the NRLMSISE-00 hydrogen density, plasmasphere, and ionosphere. *Geophysical Research Letters, 45*, 8062–8071. https://doi.org/10.1029/2018GL079206

Krall, J., Glocer, A., Fok, M.-C., Nossal, S. M., & Huba, J. D. (2018). The unknown hydrogen exosphere: Space weather implications. *Space Weather, 16*, 205–215. https://doi.org/10.1002/2017SW001780

Kutoglu, S. H., Ghasempour, F., & Sekertekin, A. (2021). Investigation of possible MODIS AOD anomalies as earthquake precursors for global earthquakes. *Advances in Space Research, 68*, 3531–3545. https://doi.org/10.1016/j.asr.2021.06.036

Le, H., Liu, J. Y., & Liu, L. (2011). A statistical analysis of ionospheric anomalies before 736 M6.0+ earthquakes during 2002–2010. *Journal of Geophysical Research, 116*, A02303. https://doi.org/10.1029/2010JA015781

Le, H., Liu, L., Liu, J. Y., Zhao, B., Chen, Y., & Wan, W. (2013). The ionospheric anomalies prior to the M9. 0 Tohoku-Oki earthquake. *Journal of Asian Earth Sciences, 62*, 476–484. https://doi.org/10.1016/j.jseaes.2012.10.034

Lee, R. F., Rolland, L. M., & Mikesell, T. D. (2018). Seismo-ionospheric observations, modeling, and backprojection of the 2016 Kaikoura earthquake. *Bulletin of the Seismological Society of America, 108*, 1794–1806.

Lejeune, R., El-Arini, M.B. (1999). An ionospheric grid algorithm for WAAS based on the minimum mean square error estimator. Proc. IES, Alexandria, VA 1–9

Lin, K., Mao, Z., Xu, Z., Dong, L., Zhang, X., Gao, Y., & Chen, C. H. (2023). Numerical solution of the atmospheric perturbations triggered by persistent lithospheric vibrations. *Remote Sensings, 15*, 3336. https://doi.org/10.3390/rs15133336

Liu, D., Zeren, Z., Huang, H., Yang, D., Yan, R., Wang, Q., Shen, X., Liu, C., & Guan, Y. (2023b). The ionospheric plasma perturbations before a sequence of strong earthquakes in Southeast Asia and Northern Oceania in 2018. *Remote Sensing, 15*(24), 5735. https://doi.org/10.3390/rs15245735

Liu, J. Y., Chen, Y. I., Chuo, Y. J., & Chen, C. S. (2006). A statistical investigation of pre-earthquake ionospheric anomaly. *Journal of Geophysical Research, 111*, A05304. https://doi.org/10.1029/2005JA011333

Liu, J. Y., Chuo, Y. J., Shan, S. J., Tsai, Y. B., Chen, Y. I., & Pulinets, S. A. (2004). Pre-earthquake ionospheric anomalies registered by continuous GPS TEC measurements. *Annales Geophysicae, 22*, 1585–1593.

Liu, J. Y., Tsai, H. F., Lin, C. H., Kamogawa, M., Chen, Y. I., Lin, C. H., Huang, B. S., Yu, S. B., & Yeh, Y. H. (2010). Coseismic ionospheric disturbances triggered by the Chi-Chi earthquake. *Journal of Geophysical Research Space Physics, 115*, A08303. https://doi.org/10.1029/2009JA014943

Liu, J., Zhang, X., Yang, X., Yang, M., Zhang, T., Bao, Z., Wu, W., Qiu, G., Yang, X., & Lu, Q. (2023a). The analysis of lithosphere–atmosphere- ionosphere coupling associated with the 2022 Luding Ms6.8 earthquake. *Remote Sensings., 15*, 4042. https://doi.org/10.3390/rs15164042

Love, J. J., & Thomas, J. N. (2013). Insignificant solar-terrestrial triggering of earthquakes. *Geophysical Research Letters, 40*, 1165–1170. https://doi.org/10.1002/grl.50211

Mahmood, I., Iqbal, M. F., Shahzad, M. I., & Qaiser, S. (2017). Investigation of atmospheric anomalies associated with Kashmir and Awaran Earthquakes. *Journal of Atmospheric and Solar-Terrestrial Physics, 154*, 75–85. https://doi.org/10.1016/j.jastp.2016.12.018

Manisalidis, I., Stavropoulou, E., Stavropoulos, A., & Bezirtzoglou, E. (2020). Environmental and health impacts of air pollution: A review. *Frontiers in Public Health, 8*, 14. https://doi.org/10.3389/fpubh.2020.00014

Maruyama, T., Tsugawa, T., Kato, H., Saito, A., Otsuka, Y., & Nishioka, M. (2011). Ionospheric multiple stratifications and irregularities induced by the 2011 off the Pacific coast of Tohoku Earthquake. *Earth, Planets and Space, 63*, 869–873.

Mavroyannis, C., & Winicler, C. (1962). The reaction of nitrogen atoms with hydrogen atoms. *Canadian Journal of Chemistry, 40*, 1–6. https://doi.org/10.1139/v62-041

Mehta, P. M., & Linares, R. A. (2017). Methodology for reduced order modeling and calibration of the upper atmosphere. *Space Weather, 15*, 1270–1287.

Mlynczak, M. G., et al. (2013). Atomic oxygen in the mesosphere and lower thermosphere derived from SABER: Algorithm theoretical basis and measurement uncertainty. *Journal of Geophysical Research Atmospheres, 118*, 5724–5735. https://doi.org/10.1002/jgrd.50401

Mlynczak, M. G., Hunt, L. A., Marshall, B. T., Mertens, C. J., Marsh, D. R., Smith, A. K., et al. (2014). Atomic hydrogen in the mesopause region derived from SABER: Algorithm theoretical basis, measurement uncertainty, and results. *Journal of Geophysical Research: Atmospheres, 119*, 3516–3526. https://doi.org/10.1002/2013JD021263

Mlynczak, M. G., & Solomon, S. (1993). A detailed evaluation of the heating efficiency in the middle atmosphere. *Journal of Geophysical Research Atmospheres, 98*(D6), 517–541. https://doi.org/10.1029/93JD00315

Moldovan, I. A., Placinta, A. O., Constantin, A. P., Moldovan, A. S., & Ionescu, C. (2012). Correlation of geomagnetic anomalies recorded at Muntele Rosu Seismic Observatory (Romania) with earthquake occurrence and solar magnetic storms. *Annales of Geophysicae-Italy, 55*(1), 125–137. https://doi.org/10.4401/ag-5367

Mukherjee, T., & Nandi, D. (2020). Review of atmospheric precursors for earthquake prediction model. In S. Kundu, U. Acharya, C. Dee, & S. Mukherjee (Eds.), *Proceedings of the 2nd International Conference on Communication, Devices and Computing. Lecture Notes in Electrical Engineering.* (Vol. 602). Singapore: Springer.

Murase, K., Kataoka, R., Nishiyama, T., Sato, K., Tsutsumi, M., Tanaka, Y., et al. (2023). Atmospheric ionizations by solar X-rays, solar protons, and radiation belt electrons in September 2017 space weather event. *Space Weather, 21*, e2023SW003651. https://doi.org/10.1029/2023SW003651

Nagamatsu, S., Maekawa, T., Ujike, Y., Hashimoto, S., & Fuke, N. (2011). The earthquake and tsunami-observations by Japanese physicians since the 11 March catastrophe. *Critical Care, 15*, 167.

Nagao, T., Orihara, Y., & Kamogawa, M. (2014). Precursory phenomena possibly related to the 2011 M9.0 off the Pacific coast of Tohoku earthquake. *Journal of Disaster Research, 9*(3), 303–310. https://doi.org/10.20965/jdr.2014.p0303

North, G. R., Pyle, J. A., & Zhang, F. (Eds.). (2014). *Encyclopedia of atmospheric sciences*. Amsterdam: Elsevier.

Nossal, S. M., Mierkiewicz, E. J., & Roesler, F. L. (2012). Observed and modeled solar cycle variation in geocoronal hydrogen using NRLMSISE-00 thermosphere conditions and the Bishop analytic exosphere model. *Journal of Geophysical Research Space Physics., 117*, 03311. https://doi.org/10.1029/2011JA017074

Odintsov, S., Boyarchuk, K., Georgieva, K., Kirov, B., & Atanasov, D. (2006). Long-period trends in global seismic and geomagnetic activity and their relation to solar activity. *Physics and Chemistry of the Earth, Parts a/b/c, 31*, 88–93. https://doi.org/10.1016/j.pce.2005.03.004

Odintsov, S. D., Ivanov-Kholodnyi, G. S., & Georgieva, K. (2007). Solar activity and global seismicity of the earth. *Bulletin of the Russian Academy of Science Physics, 71*, 593–595. https://doi.org/10.3103/S1062873807040466

Ohta, K., Izutsu, J., Schekotov, A., & Hayakawa, M. (2013). The ULF/ELF electromagnetic radiation before the 11 March 2011 Japanese earthquake. *Radio Science, 48*, 589–596. https://doi.org/10.1002/rds.20064

Oikonomou, C., Haralambous, H., Pulinets, S., Khadka, A., Paudel, S. R., Barta, V., Muslim, B., Kourtidis, K., Karagioras, A., & İnyurt, S. (2021). Investigation of pre-earthquake ionospheric and atmospheric disturbances for three large earthquakes in Mexico. *Geosciences, 11*, 16. https://doi.org/10.3390/geosciences11010016

Orihara, Y., Kamogawa, M., & Nagao, T. (2014). Preseismic changes of the level and temperature of confined groundwater related to the 2011 Tohoku Earthquake. *Science and Reports, 4*, 6907. https://doi.org/10.1038/srep06907

Oyama, K. I., Chen, C. H., Bankov, L., Minakshi, D., Ryu, K., Liu, J. Y., & Liu, H. (2019). Precursor effect of March 11, 2011 off the coast of Tohoku earthquake on high and low latitude ionospheres and its possible disturbing mechanism. *Advances in Space Research, 63*(8), 2623–2637. https://doi.org/10.1016/j.asr.2018.12.042

Ozawa, S., Nishimura, T., Suito, H., et al. (2011). Coseismic and postseismic slip of the 2011 magnitude-9 Tohoku-Oki earthquake. *Nature, 475*, 373–376. https://doi.org/10.1038/nature10227

Paine, C. G., & Seidel, G. M. (1994). The adsorption of helium on liquid hydrogen. *Physica b: Condensed Matter, 194–196*, 969–970. https://doi.org/10.1016/0921-4526(94)90814-1

Parrot, M., Berthelier, J. J., Lebreton, J. P., Sauvaud, J. A., Santolik, O., & Blecki, J. (2006). Examples of unusual ionospheric observations made by the DEMETER satellite over seismic regions. *Physics and Chemistry of the Earth Parts, a/b/c, 31*(4–9), 486–495.

Pederick, L., & Cervera, M. (2014). Semiempirical model for ionospheric absorption based on the NRLMSISE-00 atmospheric model. *Radio Science, 49*, 81–93. https://doi.org/10.1002/2013RS005274

Perez, D., & Bevilacqua, R. (2015). Neural Network based calibration of atmospheric density models. *Acta Astronautica, 110*, 58–76.

Perrone, L., Korsunova, L. P., & Mikhailov, A. V. (2010). Ionospheric precursors for crustal earthquakes in Italy. *Annales Geophysicae, 28*, 941–995. https://doi.org/10.5194/angeo-28-941-2010

Picone, J. M., Hedin, A. E., Drob, D. P., & Aikin, A. C. (2002). NRLMSISE-00 empirical model of the atmosphere: Statistical comparisons and scientific issues. *Journal of Geophysical Research Space Physics, 107*, 15–16.

Picozza, P., Conti, L., & Sotgiu, A. (2021). Looking for earthquake precursors from space: A critical review. *Frontiers in Earth Science, 9*, 676775. https://doi.org/10.3389/feart.2021.676775

Pinault, J.-L., & Baubron, J.-C. (1996). Signal processing of soil gas radon, atmospheric pressure, moisture, and soil temperature data: A new approach for radon concentration modeling. *Journal of Geophysical Research, 101*(B2), 3157. https://doi.org/10.1029/95JB03121

Piscini, A., De Santis, A., Marchetti, D., & Cianchini, G. (2017). A multi-parametric climatological approach to study the 2016 Amatrice-Norcia (Central Italy) Earthquake Preparatory Phase. *Pure and Applied Geophysics, 174*(10), 3673–3688. https://doi.org/10.1007/s00024-017-1597-8

Price, C., Plotnik, T., Saha, J., & Guha, A. (2023). Revisiting the link between thunderstorms and upper tropospheric water vapor. *Journal of Geophysical Research Atmospheres, 128*, e2023JD039306. https://doi.org/10.1029/2023JD039306

Pulinets, S. (2011). The synergy of earthquake precursors. *Earthquake Science, 24*(6), 535–548. https://doi.org/10.1007/s11589-011-0815-1

Pulinets, S. A., & Boyarchuk, K. A. (2004). *Ionospheric precursors of earthquakes* (p. 315). Berlin: Springer.

Pulinets, S., & Budnikov, P. (2022). Atmosphere critical processes sensing with ACP. *Atmosphere, 13*, 1920. https://doi.org/10.3390/atmos13111920

Pulinets, S. A., Ouzounov, D. P., Karelin, A. V., et al. (2015). Physical bases of the generation of short-term earthquake precursors: A complex model of ionization-induced geophysical processes in the lithosphere-atmosphere-ionosphere-magnetosphere system. *Geomagnetizm i Aeronomiya, 55*, 521–538. https://doi.org/10.1134/S0016793215040131

Pulinets, S., Ouzounov, D., Karelin, A., & Boyarchuk, K. (2022). *Earthquake precursors in the ionosphere*. Springer, Dordrecht: Earthquake precursors in the atmosphere and ionosphere. https://doi.org/10.1007/978-94-024-2172-9_3

Pulinets, S. A., Ouzounov, D., Karelin, A. V., Boyarchuk, K. A., & Pokhmelnykh, L. A. (2006). The physical nature of thermal anomalies observed before strong earthquakes. *Physics and Chemistry of the Earth, Parts a/b/c, 31*(4–9), 143–153. https://doi.org/10.1016/j.pce.2006.02.042

Pulinets, S., Ouzounov, D., Karelin, A., & Davidenko, D. (2018). Lithosphere-atmosphere-ionosphere-magnetosphere coupling a concept for pre-earthquake signals generation. In D. Ouzounov, S. Pulinets, K. Hattori, & P. Taylor (Eds.), *Pre-earthquake processes: a multidisciplinary approach to earthquake prediction studies* (pp. 77–98). USA: Wiley.

Qian, L., Burns, A. G., Solomon, S. S., Smith, A. K., McInerney, J. M., et al. (2018). Temporal variability of atomic hydrogen from the mesopause to the upper thermosphere. *Journal of Geophysical Research: Space Physics, 123*, 1006–1017.

Qin, J., & Waldrop, L. (2016). Non-thermal hydrogen atoms in the terrestrial upper thermosphere. *Nature Communications, 7*(1), 13655. https://doi.org/10.1038/ncomms13655

Qin, K., Zheng, S., Wu, L., et al. (2021). Quasi-synchronous multi-parameter anomalies before Wenchuan and Yushu earthquakes in China. *The European Physical Journal Special Topics, 230*, 263–274. https://doi.org/10.1140/epjst/e2020-000253-3

Reber, C. A., Hedin, A. E., & Chandra, S. (1973). Equatorial phenomena in neutral thermospheric composition. *Journal of Atmospheric and Terrestrial Physics, 35*, 6. https://doi.org/10.1016/0021-9169(73)90019-6

Rey-Pommier, A., Chevallier, F., Ciais, P., Kushta, J., Christoudias, T., Bayram, I. S., & Sciare, J. (2023). Detecting nitrogen oxide emissions in Qatar and quantifying emission factors of gas-fired power plants—A 4-year study. *Atmospheric Chemistry and Physics, 23*, 13565–13583. https://doi.org/10.5194/acp-23-13565-2023

Ryu, K., Oyama, K. I., Bankov, L., Chen, C. H., Devi, M., Liu, H., & Liu, J. Y. (2016). Precursory enhancement of EIA in the morning sector: Contribution from mid-latitude large earthquakes in the north-east Asian region. *Advances in Space Research, 57*, 268–280.

Sahithi, K., Venkata, R., & Kumar, D. (2019). Ionospheric time delay corrections based on the extended single layer model over low latitude region. *Geodesy and Geodynamics, 10*, 235–240.

Saito, A., Tsugawa, T., Otsuka, Y., Nishioka, M., Iyemori, T., Matsumura, M., Saito, S., Chen, C., Goi, Y., & Choosakul, N. (2011). Acoustic resonance and plasma depletion detected by

GPS total electron content observation after the 2011 off the Pacific coast of Tohoku Earthquake. *Earth, Planets and Space, 63*, 863–867.

Sano, Y., Hara, T., Takahata, N., et al. (2014). Helium anomalies suggest a fluid pathway from mantle to trench during the 2011 Tohoku-Oki earthquake. *Nature Communications, 5*, 3084. https://doi.org/10.1038/ncomms4084

Sano, Y., Nakamura, Y., Wakita, H., & Urabe, A. (1984). Tominaga, T. Helium-3 emission related to volcanic activity. *Science, 224*, 150–151.

Satti, M. S., Ehsan, M., Abbas, A., Shah, M., FranciscodeOliveira-Júnior, J., & Naqvi, N. A. (2022). Atmospheric and ionospheric precursors associated with M w ≥ 6.5 earthquakes from multiple satellites. *Journal of Atmospheric Solar-Terrestial Physics, 227*, 105802. https://doi.org/10.1016/j.jastp.2021.105802

Seemala, G. K. (2023). Estimation of ionospheric total electron content (TEC) from GNSS observations. *Atmospheric remote sensing* (pp. 63–84). Amsterdam: Elsevier. https://doi.org/10.1016/B978-0-323-99262-6.00022-5

Seno, T., Sakurai, T., & Stein, S. (1996). Can the Okhotsk plate be discriminated from the North American plate? *Journal of Geophysical Research, 101*, 11305–11315. https://doi.org/10.1029/96JB00532

Shah, M. (2022). Earthquake ionospheric and atmospheric anomalies from GNSS TEC and other satellites. *Computers in earth and environmental sciences* (pp. 399–387). Amsterdam: Elsevier. https://doi.org/10.1016/B978-0-323-89861-4.00009-9

Shah, M., Ahmed, A., Ehsan, M., Khan, M., Tariq, M. A., Calabia, A., & Rahman, Z. (2020c). Total electron content anomalies associated with earthquakes occurred during 1998–2019. *Acta Astronautica, 175*, 268–276.

Shah, M., Calabia, A., Tariq, M. A., Ahmed, J., & Ahmed, A. (2020a). Possible ionosphere and atmosphere precursory analysis related to Mw-6.0 earthquakes in Japan. *Remote Sensing of Environment, 239*, 111620.

Shah, M., Inyurt, S., Ehsan, M., Ahmed, A., Shakir, M., Ullah, S., & Iqbal, M. S. (2020b). Seimo ionospheric anomalies in Turkey associated with Mw ≥ 6.0 earthquakes detected by GPS TEC and GIM TEC. *Advances in Space Research, 65*, 2540–2550.

Shah, M., & Jin, S. (2018). Pre-seismic ionospheric anomalies of the 2013 Mw = 7.7 Pakistan earthquake from GPS and COSMIC observations. *Geodesy and Geodynamics, 9*, 378–387. https://doi.org/10.1016/j.geog.2017.11.008

Shah, M., Qureshi, R. U., Khan, N. G., Ehsan, M., & Yan, J. (2021). Artificial neural network based thermal anomalies associated with earthquakes in Pakistan from MODIS LST. *Journal of Atmospheric and Solar-Terrestrial Physics, 215*, 105568.

Shah, M., Tariq, M. A., Ahmad, J., Naqvi, N. A., & Jin, S. (2019). Seismo ionospheric anomalies before the 2007 M7.7 Chile earthquake from GPS TEC and DEMETER. *Journal of Geodynamics, 127*, 42–51.

Shao, X., Ho, S.-P., Jing, X., Zhou, X., Chen, Y., Liu, T.-C., Zhang, B., & Dong, J. (2023). Characterizing the tropospheric water vapor spatial variation and trend using 2007–2018 COSMIC radio occultation and ECMWF reanalysis data. *Atmospheric Chemistry and Physics, 23*, 14187–14218. https://doi.org/10.5194/acp-23-14187-2023

Sharzehei, M., Masnadi-Shirazi, M. A., & Golbahar-Haghighi, Sh. (2015). Statistical investigation of the noise added to a model of the effect of solar activities on the plasma of the ionosphere using DEMETER satellite data. *Journal of Atmospheric and Solar-Terrestrial Physics, 130–131*, 172–181. https://doi.org/10.1016/j.jastp.2015.05.011

Sherwood, S. C., Roca, R., Weckwerth, T. M., & Andronova, N. G. (2010). Tropospheric water vapor, convection, and climate. *Reviews of Geophysics., 48*, RG2001. https://doi.org/10.1029/2009RG000301

Shi, C., Li, W., Min, L., Zhao, Q., & Sang, J. (2015). Calibrating the scale of the NRLMSISE00 model during solar maximum using the two line elements dataset. *Advances in Space Research, 56*, 1–9.

Shin, H., & Kwon, Y. (2012). Commensurate-incommensurate transition of 4 He adsorbed on a single C60 molecule. *The Journal of Chemical Physics, 136*, 064514.

Simpson, J. (2008). Global FDTD Maxwell's equations modeling of electromagnetic propagation from currents in the lithosphere. *IEEE Transactions on Antennas and Propagation, 56*, 1199–1203. https://doi.org/10.1109/TAP.2007.913149

Smirnov, B.M. (2017). Infrared atmospheric emission. in *Microphysics of atmospheric phenomena*. (Springer, Cham) https://doi.org/10.1007/978-3-319-30813-5

Sobolev, G. A. (2021). The effect of strong magnetic storms on the occurrence of large earthquakes. *Izvestiya, Physics of the Solid Earth, 57*(1), 20–36. https://doi.org/10.31857/S0002333721010087

Sobolev, G. A., & Zakrzhevskaya, N. A. (2020). Local tectonic deformations and nearby contemporaneous earthquakes. *Journal of Volcanology and Seismology, 14*, 137–144. https://doi.org/10.1134/S0742046320030070

Sparks, L., Lijima, B. A., Mannucci, A. J., Pi, X., Wilson, B.D. (2000). A new model for retrieving slant TEC corrections for wide area differential GPS, in: 2000: Navigating into the New Millennium Technical Meeting. Anaheim CA United States pp. 464–473

Sukma, I., & Abidin, Z. Z. (2017). Study of seismic activity during the ascending and descending phases of solar activity. *Indian Journal of Physics, 91*, 595–606. https://doi.org/10.1007/s12648-016-0943-5

Swati, B. S., Pundhir, D., Ashwini, K. S., Madhusudan, R., Anirban, G., & Yashuhide, H. (2020). Ultra-low frequency (ULF) magnetic field emissions associated with some major earthquakes occurred in Indian Subcontinent. *Journal of Atmospheric and Solar-Terrestrial Physics, 211*, 105469. https://doi.org/10.1016/j.jastp.2020.105469

Takla, E. M. H., & Samwel, S. W. (2023). Possible connection between solar activity and local seismicity. *Terrestial, Atmospheric and Oceanic Science, 34*, 9. https://doi.org/10.1007/s44195-023-00042-6

Tariq, M. A., Shah, M., Inyurt, S., Shah, M. A., & Liu, L. (2020). Comparison of TEC from IRI-2016 and GPS during the low solar activity over Turkey. *Astrophysics and Space Science., 365*, 179. https://doi.org/10.1007/s10509-020-03894-3

Temmer, M. (2021). Space weather: The solar perspective. *Living Reviews in Solar Physics, 18*, 4. https://doi.org/10.1007/s41116-021-00030-3

Tronin, A. A. (2006). Remote sensing and earthquakes: A review. *Physics and Chemistry of the Earth Parts a/b/c, 31*(4–9), 138–142. https://doi.org/10.1016/j.pce.2006.02.024

Tsugawa, T., Saito, A., Otsuka, Y., Nishioka, M., Maruyama, T., Kato, H., Nagatsuma, T., & Murata, K. (2011). Ionospheric disturbances detected by GPS total electron content observation

after the 2011 off the Pacific coast of Tohoku Earthquake. *Earth, Planets and Space, 63*, 875–879.

Urata, N., Duma, G., & Freund, F. (2018). Geomagnetic Kp index and earthquakes. *Open Journal of Earthquake Research, 7*, 39–52. https://doi.org/10.4236/ojer.2018.71003

Vainio, R., Desorgher, L., Heynderickx, D., et al. (2009). Dynamics of the earth's particle radiation environment. *Space Science Reviews, 147*, 187–231. https://doi.org/10.1007/s11214-009-9496-7

Wallace, J., Hobbs, P. (2006). *Atmospheric Science An Introductory Survey* (2nd ed., pp. 44–483). International Geophysics Series. https://doi.org/10.5860/choice.44-3925

Walsh, C. R., & TimothyPatterson, R. (2022). Precipitation and temperature trends and cycles derived from historical 1890–2019 weather data for the city of Ottawa, Ontario, Canada. *Environments, 9*(3), 35. https://doi.org/10.3390/environments9030035

Walter, T., Hansen, A., Blanch, J., Enge, T., Mannucci, X., Sparks, L., Iijma, B., El-Arini, M., Lejeune, R., Hagen, M., ltshular, E., Fries, R., Chu, A. (2000). Robust detection of ionosphere irregularities. Proc. Inst. Navig. Annu. Meeting, Salt Lake City, UT, pp. 209–218

Wang, W., & Hocke, K. (2022). Atmospheric effects and precursors of rainfall over the Swiss Plateau. *Remote Sensing, 14*(12), 2938. https://doi.org/10.3390/rs14122938

Wang, Z., Ni, Z., Chen, S., Su, S., & Yuan, J. (2022). Characteristics of local geomagnetic field variations and the tectonic stress field adjacent to the 21 May 2021, Ms 6.4 Yangbi Earthquake, Yunnan China. *Applied Sciences, 12*, 1005. https://doi.org/10.3390/app12031005

Woith, H. (2015). Radon earthquake precursor: a short review. *European Physical Journal Special Topics, 224*(4), 611–627. https://doi.org/10.1140/epjst/e2015-02395-9

Xiong, C., Lühr, H., Schmidt, M., Bloßfeld, M., & Rudenko, S. (2018). An empirical model of the thermospheric mass density derived from CHAMP satellite. *Ann Geophys Ger, 36*, 1141–1152.

Xu, G., Han, P., Huang, Q., Hattori, K., & Febriani, Y. H. (2013). Anomalous behaviors of geomagnetic diurnal variations prior to the 2011 off the Pacific coast of Tohoku earthquake (Mw9.0). *Journal of Asian Earth Sciences, 77*, 59–65. https://doi.org/10.1016/j.jseaes.2013.08.011

Yanchukovsky, V. L. (2020). Solar activity and Earth seismicity. *Solar Terrestrial Physics, 6*(4), 67–77. https://doi.org/10.12737/stp71202109

Yang, H., Moreno, E. M., & Hernández-Pajares, M. (2019a). ADDTID: an alternative tool for studying earthquake/tsunami signatures in the ionosphere. Case of the 2011 Tohoku Earthquake. *Remote Sensing, 11*, 1894. https://doi.org/10.3390/rs11161894

Yang, S. S., Asano, T., & Hayakawa, M. (2019b). Abnormal gravity wave activity in the stratosphere prior to the 2016 Kumamoto earthquakes. *Journal of Geophysical Research: Space Physics, 124*, 1410–1425. https://doi.org/10.1029/2018JA026002

Yesugey, S. C. (2009). Comparative evaluation of the influencing effects of geomagnetic solar storms on earthquakes in Anatolian Peninsula. *Earth Sciences Research Journal, 13*, 82–89.

Zawdie, K., Belehaki, A., Burleigh, M., Chou, M.-Y., Dhadly, M. S., Greer, K., Halford, A. J., Hickey, D., Inchin, P., Kaeppler, S. R., Klenzing, J., Narayanan, V. L., Sassi, F., Sivakandan, M., Smith, J. M., Zabotin, N., Zettergren, M. D., & Zhang, S.-R. (2022). Impacts of acoustic and gravity waves on the ionosphere. *Frontiers in Astronomy and Space Science., 9*, 1064152. https://doi.org/10.3389/fspas.2022.1064152

Zedek, F., Rolland, L. M., Mikesell, T. D., et al. (2021). Locating surface deformation induced by earthquakes using GPS, GLONASS and Galileo ionospheric sounding from a single station. *Advances in Space Research, 68*, 3403–3416. https://doi.org/10.1016/j.asr.2021.06.011

Zhang, H., Gu, D., Duan, X., & Wei, C. (2018). Atmospheric density model calibration using emperical orthogonal function. *Acta Aeronautica. Astronautica Sinica, 39*, 722263.

Zhang, Y., Yu, J., Chen, J., & Sang, J. (2021). An empirical atmospheric density calibration model based on long short-term memory neural network. *Atmosphere, 12*, 925. https://doi.org/10.3390/atmos12070925

Zhou, H., Yan, F., Wang, J., Luo, Q., & Jin, T. (2021). Study on the ULF magnetic field generated by Earth currents relating to large EQs. *Radio Science, 56*, e2019RS006992. https://doi.org/10.1029/2019RS006992

Zhou, Y., Yang, J., Zhu, F., Su, F., Hu, L., & Zhai, W. (2017). Ionospheric disturbances associated with the 2015 M7. 8 Nepal earthquake. *Geodesy and Geodynamics*, *8*(4), 221–228. https://doi.org/10.1016/j.geog.2017.04.004

Zhu, J., Sun, K., & Zhang, J. (2023). Anomalies in infrared outgoing longwave radiation data before the Yangbi Ms6.4 and Luding Ms6.8 earthquakes based on time series forecasting models. *Applied Sciences, 13*, 8572. https://doi.org/10.3390/app13158572

(Received August 1, 2023, revised February 13, 2024, accepted March 19, 2024)